Electrochimica Acta 101 (2013) 41–58

Contents lists available at SciVerse ScienceDirect

Electrochimica Acta

journal homepage: www.elsevier.com/locate/electacta

Review

Model catalyst studies on hydrogen and ethanol oxidation for fuel cells

Jochen Friedl[a,b], Ulrich Stimming[a,b,c,*,1]

[a] TUM CREATE Centre for Electromobility, 1 CREATE Way, CREATE Tower, Singapore 138602, Singapore
[b] Department of Physics E19, Technische Universität München, James-Franck Str. 1, 85748 Garching, Germany
[c] Institute for Advanced Study (IAS) of the Technische Universität München, Lichtenbergstr. 2a, 85748 Garching, Germany

ARTICLE INFO

Article history:
Received 16 July 2012
Received in revised form
28 December 2012
Accepted 30 December 2012
Available online 6 January 2013

Keywords:
Model catalyst
Nanostructures
Activity
Fuel cell system
Direct ethanol fuel cell

ABSTRACT

Fuel cells are considered a possible option for future automotive applications. They chemically convert a multitude of different energy carriers to electricity and are not limited by the Carnot-efficiency. This review investigates the ethanol oxidation reaction which takes place at the anode of a direct ethanol fuel cell (DEFC). Reaction pathways under different conditions, in acid and alkaline media, are reported. Special focus lies on the CO_2 current efficiency (CCE) which is important for the overall efficiency of the fuel cell. The present C—C bond is the biggest challenge for achieving a total oxidation from ethanol to CO_2. Reported results are promising, with CCEs higher than 80%. In order to further enhance reaction kinetics the DEFC can be operated at higher temperatures, e.g. 200–400 °C. This requires a new and more temperature resilient membrane. Ammonium polyphosphate composites are suitable materials which show good conductivity and high thermal stability up to approximately 250 °C. As a benchmark system for catalyst research this review discusses achievements of model catalyst studies on nanostructured surfaces for hydrogen related reactions. By carefully designing support and catalyst nanoparticles specific exchange current densities more than four orders of magnitude higher than for bulk platinum were realized. For ethanol oxidation model catalyst studies were performed too. Studies aiming at understanding the influence of coordination, particle size, substrate, composition and alloying of catalyst particles on the ethanol oxidation are presented. Catalysts at elevated temperatures are also within the scope of this review.

Contents

1. Introduction 41
2. Direct ethanol fuel cell 43
 2.1. Ethanol oxidation reaction in acidic media 43
 2.2. Ethanol oxidation reaction in alkaline media 44
 2.3. Intermediate temperature direct ethanol fuel cells membranes 46
3. Model catalyst research 47
 3.1. Creating nanostructured model surfaces 48
 3.2. Reactivity measurements 49
4. Model catalyst research for the ethanol oxidation reaction 50
 4.1. Acid media 51
 4.2. Alkaline media 52
 4.3. Catalysts at elevated temperatures 53
5. Conclusions 54
 References 55

1. Introduction

At the moment mankind is facing two major boundary conditions in conjunction with the use of energy: resources and climate. In terms of resources there is a discrepancy between demand and supply of some primary energy carriers. For the climate it is the fact

* Corresponding author at: TUM CREATE Centre for Electromobility, 1 CREATE Way, CREATE Tower, Singapore 138602, Singapore. Tel.: +65 65923013; fax: +65 68969950.
E-mail address: ulrich.stimming@tum-create.edu.sg (U. Stimming).
[1] ISE member.

0013-4686/$ – see front matter © 2013 Elsevier Ltd. All rights reserved.
http://dx.doi.org/10.1016/j.electacta.2012.12.130

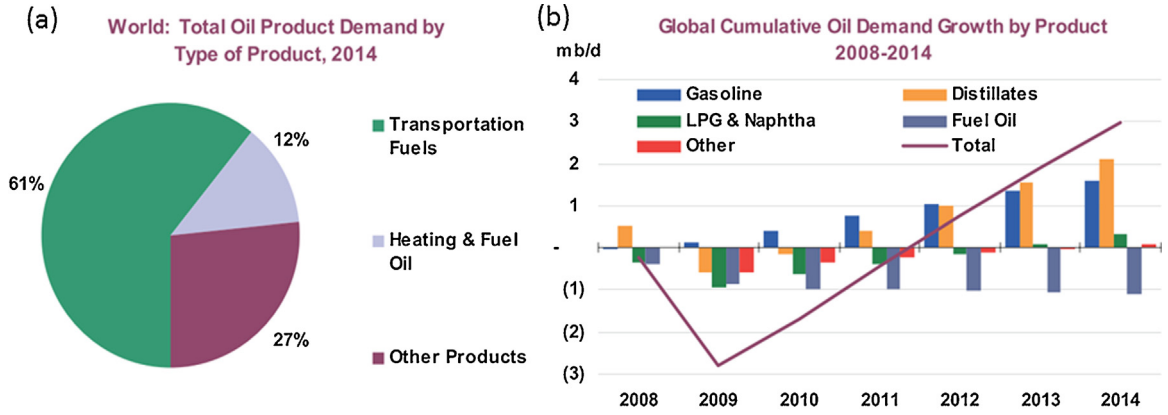

Fig. 1. (a) Extrapolated total oil product demand in 2014 by type of product. (b) Trend of global cumulative oil demand growth in million barrels per day (mb/d). Reprinted from [1].

that the release of green-house gases increases the temperature of our planet's atmosphere.

According to an extrapolation calculated by the International Energy Agency (IEA) the growing demand for oil is spearheaded by the need for transportation fuel in the nearest future [1]. While in OEDC countries the hunger for gasoline, diesel and jet fuel can be somewhat cushioned by a structural decline in burning fuels and industrial feedstock, non-OECD countries will combust more products made from crude oil. This will lead to a global cumulative oil demand growth as depicted in Fig. 1(b). Transportation will account for 61% percent of the total demand for oil products in 2014; details are given in Fig. 1(a).

As it is questionable how long the oil producing countries can satisfy growing demands, leaving aside political instabilities and rising prices, it seems necessary to look for an alternative source of fuel. Ideally this fuel would be renewable, could be produced without interfering with the food chain, combines high energy density with non-toxicity, is easy to transport and could be distributed making use of existing infrastructure.

The other boundary for the future of transportation is the climate of our planet. In Energy Technology Perspectives 2012 (ETP 2012) the IEA presents several scenarios for the future. The 2 °C scenario (2DS) requires a reduction of more than 50% for all energy related CO_2 emissions in the year 2050 compared to CO_2 emissions in 2009. Latest climate research indicates that this would limit the global temperature rise to 2 °C with a high probability (80%) [2]. In Fig. 2 the target point of the globally emitted mass of CO_2 to reach this benign scenario 2DS is compared to the emissions leading to scenario 6DS. Scenario 6DS comprises a rise in global temperature of 6 °C in the year 2050. In order to achieve ETP 2012 2DS all sectors, including transportation, must reduce their emissions drastically. For transport the emitted gram of CO_2 per driven kilometer for private light duty vehicles (PLDVs) is given in Table 1. Simply improving efficiency of internal combustion engines (ICE) will not suffice to reach the 2DS objectives [2]. Therefore, another property of future fuel, dictated by the boundary climate, has to be low CO_2 emissions per driven kilometer.

Table 1
Enacted and proposed standards for vehicle fuel economy for new private light duty vehicles (PLDVs) in terms of emission of gCO_2/km. The data for the United States and Canada comprises light-commercial vehicles, SUVs and passenger vehicles. Values are extracted from [2].

	Average new PLDV fuel economy/(gCO_2/km)			
	2010	2015	2020	2025
Japan	125	127	103	n.a.
EU	142	132	113	95
Canada	178	158	n.a.	n.a.
China	183	165	n.a.	n.a.
Korea	183	142	n.a.	n.a.
USA	192	165	133	102
Australia	217	n.a.	n.a.	n.a.

One of the few options for this new fuel is ethanol oxidized in a fuel cell (FC). FCs are not limited by the Carnot efficiency which ICEs cannot overcome [3]; they can convert chemical energy with fewer losses. As ethanol is a liquid hydrocarbon, just like gasoline, it could be disseminated via existing infrastructure. Furthermore it is non-toxic and does not require advanced mobile storage containers as it is the case with compressed or liquefied H_2. In addition it can be produced by sustainable routes [2]. Compared to other energy vectors converted in FCs the energy density of ethanol is high. Fig. 3 depicts how favorably ethanol compares to other energy carriers which can be converted in FCs [4,5]. Only metal hydrides lead to higher stored volumetric H_2 density. However, those solid-state

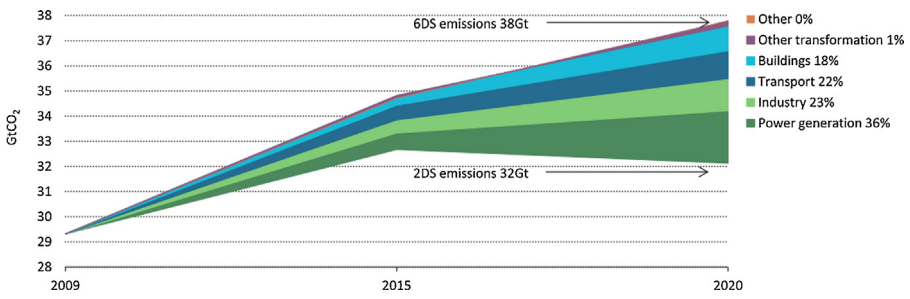

Fig. 2. Global emissions and derrived future emission of CO_2 in gigatonnes (Gt) listed by contributing sectors.

Reprinted from [2].

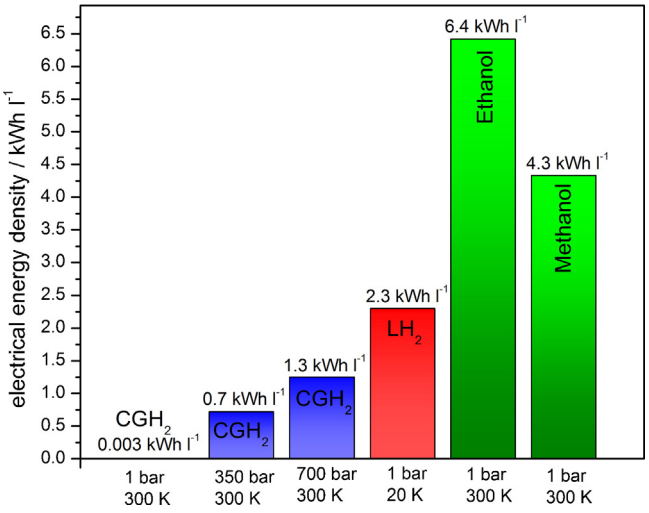

Fig. 3. Volumetric electrical energy density in kWh/l for different fuels multiplied by the thermodynamic efficiency of a fuel cell. Numbers for hydrogen atoms per cm^{-3} for compressed gaseous hydrogen (CGH_2) and liquid hydrogen (LH_2) are taken from [6]. Thermodynamic efficiencies of 83% for hydrogen/oxygen conversion and 96% for methanol/oxygen and ethanol/oxygen conversion are assumed [19].

absorbers suffer not only from heavy weight but also influence the FC with their kinetics and they are still far from meeting the aimed target for their transport applications [6–9]. In addition, generation of hydrogen from electricity via electrolysis of water suffers from the low system efficiency (60–73%) of commercial electrolyzers [10].

On the other hand hydrogen could be reformed from hydrocarbons and alcohols (e.g. ethanol) on board. While hydrogen production is common place in the chemical industry and some interesting biotechnological advances were made [11,12], it is more demanding for mobile applications because of issues such as weight, size, transient operation and consumer safety [13]. Moreover, proton exchange membrane fuel cells (PEMFCs) require a supply of almost pure H_2. Especially the CO content in the fuel has to be low (<20 ppm), to avoid poisoning of the anode catalyst [14]. In order to obtain hydrogen with such purity selective processing that involves multiple reforming steps and cleaning are necessary, if it is reformed on-board [15]. While demonstrator vehicles with on-board reforming were realized, Daimler Chrysler's Necar 5 for example featured a very sophisticated methanol reformer [16], the required high degree of integration is demanding and also leads to high costs [17,18]. The array of fuel processors which is necessary to extract hydrogen from hydrocarbons was referred to as a mobile 'small chemical plant' [17].

Therefore, we would like to focus on direct ethanol fuel cells (DEFCs). These oxidize ethanol directly at the anode which allows for a simpler design. PEMFCs as well as anion exchange membrane fuel cells (AEMFCs) yield promising CO_2 current efficiencies (CCEs) when fed with ethanol as will be shown in Section 2. However, the reaction mechanism of the ethanol oxidation reaction (EOR) is not straightforward and we will review the current knowledge of the reaction pathway both in acidic and alkaline media. The related question of a suitable membrane for intermediate temperatures will be addressed in this section too. To motivate the quest for an advanced catalyst material, which can effectively cleave the C—C bond of ethanol, we present in Section 3 how experimental realization of model catalysts in interplay with extensive theoretical work broadened fundamental understanding of the hydrogen evolution reaction (HER) and hydrogen oxidation reaction (HOR). Section 4 applies the methods of model catalyst studies to the EOR both in alkaline and acid media to take stock what has been done so far to improve the catalytic activity toward the total oxidation of ethanol.

2. Direct ethanol fuel cell

Instead of converting ethanol to hydrogen in a reforming step it is possible to directly feed ethanol to the anode of a DEFC. This adds the benefit of a simple design for mobile applications to the benign properties of ethanol as energy carrier. Fig. 4 shows a sketch of a DEFC working at elevated temperatures in acidic conditions. However, the C—C bond in ethanol leads to a rather complicated reaction mechanism and formation of intermediates like acetaldehyde and acetic acid [20–24]. Since the ultimate challenge for DEFC is to speed up the sluggish kinetics and to increase the CCE of the EOR, a detailed understanding of the reaction pathway is essential. Besides intensive studies in acidic media the EOR was also studied in alkaline environments, which show a high concentration of OH_{ads}— groups. These assist in the removal of electrode poisoning species CO_{ads} [25].

A brief glance at one of the experimental results described in Section 2.1 allows validating the DEFC sketch shown in Fig. 4. Shimada et al. obtained a current efficiency of total oxidation of ethanol of more than 80% in their membrane electrode assembly, while feeding an anolyte with a molar water to ethanol mixture of 3:1 at a temperature of 250 °C [26]. At the cathode of a DEFC 6 mol of water are produced per mole of ethanol under uptake of 3 mol of H_2O. This allows recuperating the H_2O needed in the anode reaction from the exhaust gas. The overall chemical reaction for a DEFC is given in Eq. (1):

$$CH_3CH_2OH + 3O_2 \rightarrow 2CO_2 + 3H_2O \quad (1)$$

2.1. Ethanol oxidation reaction in acidic media

It is known that the EOR follows a multistep mechanism with a number of adsorbed reaction intermediates and a possible formation of by-products which diminish electron yield and lead to undesired substances [21,22]. To elucidate the exact mechanism the EOR in acid environment was investigated by means of differential electrochemical mass spectroscopy (DEMS) [24,27–31], Fourier transform infrared spectroscopy (FTIR) [22,31–35], gas chromatography (GC), high performance liquid chromatography (HPLC) [23,26,36,37] or, more recently, liquid state nuclear magnetic resonance spectroscopy (NMR) [20].

Eq. (2) gives the main reaction how electrical energy stored in ethanol providing 12 electrons is extracted:

$$CH_3CH_2OH + 3H_2O \rightarrow 2CO_2 + 12H^+ + 12e^- \quad (2)$$

In order to achieve a high activity for the EOR the C—C and C—H bonds need to be cleaved [28]. Otherwise one of the partial oxidations given in Eqs. (3–5) takes place:

$$CH_3CH_2OH \rightarrow CH_3CHO + 2H^+ + 2e^- \quad (3)$$

$$CH_3CH_2OH + H_2O \rightarrow CH_3CH(OH)_2 + 2H^+ + 2e^- \quad (4)$$

$$CH_3CH_2OH + H_2O \rightarrow CH_3CHOOH + 4H^+ + 4e^- \quad (5)$$

The oxidations to acetaldehyde (AAL) described in Eq. (3) and the one to ethane-1,1-diol (ED), shown in Eq. (4), release two electrons. Acetic acid (AA) is formed from ethanol with water under exchange of four electrons with an electrode (Eq. (5)). Formation of any of these unwanted by-products results in a significant decrease of the exploitable energy content of 8 kWh/kg [24]. Recently, Kim et al. published an extensive chart showing the electrochemical reaction pathways of ethanol on 40 wt.% Pt/C catalysts based on their own ^{13}C liquid-state NMR experimental work as well as publications by several other groups [20]. The authors reported that the first

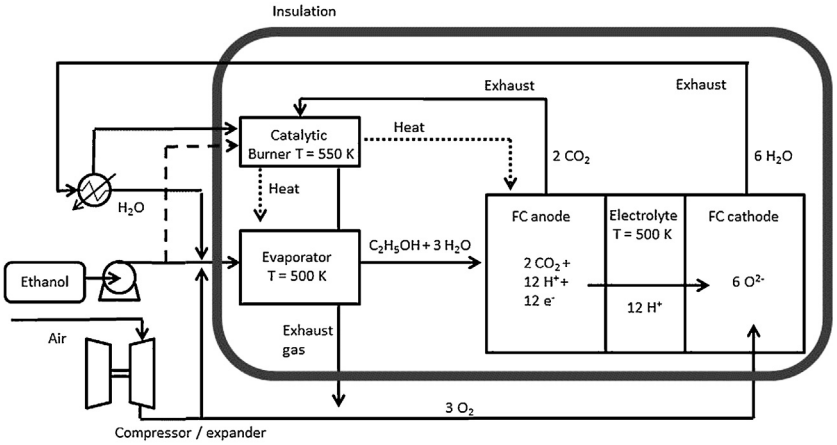

Fig. 4. Possible design for a DEFC system in acid medium. No reforming is necessary which makes a compact design feasible. Solid arrows represent material flow while dotted arrows stand for heat flow. The dashed line depicts an additional feed of ethanol to the catalytic burner which can be activated, if required by the operation conditions of the fuel cell.

step of ethanol adsorption and oxidation on Pt is the formation of Pt—OCH_2—CH_3 and Pt—CHOH—CH_3 which confirms earlier findings [32,38]. When these species are transformed to Pt—CO—CH_3 and Pt—CO they can be oxidized to CH_3COOH or CO_2. Oxygen containing species, such as OH_{ads}, play a key role in the various oxidation reactions [20,39,40].

What fraction of the gaseous ethanol is ultimately converted to CO_2 is influenced by a multitude of different parameters such as ethanol concentration, pressure, temperature, applied potential and choice of catalyst.

Studies performed within the last two decades reported a wide spectrum of CO_2 yields for the EOR. Some representative publications and their key findings are briefly presented in Table 2.

In their studies at polycrystalline Pt conducted at room-temperature Camara and Iwasita found that the concentration of ethanol supplied to the anode has a major influence on the reaction pathway of the EOR, whether AA or AAL is the main by-product [34]. High yields for the four electrons releasing oxidation to AA and the total oxidation to CO_2 were only observed at ethanol concentrations below 0.1 M. With increasing ethanol concentration oxidation to AAL becomes the main reaction. This change in product was also reported by other groups [22,28] and Camara and Iwasita proposed that the inhibition of CO_2 and AA is caused by reduction of reaction sites for water adsorption by adsorbed ethanol [34].

The highest CO_2 yields of Table 2 are reported for membrane electrode assemblies (MEAs) and not for model electrodes [26,36,41]. Rao et al. proposed that the intrinsic anodic oxidation conditions within a PEMFC anode, mainly residence time and catalyst loading, enhance the C—C cleavage rate [41]. As shown in Fig. 5(a), which depicts the CCE as a function of temperature and applied potential, they could achieve almost total oxidation of EtOH to CO_2 in their setup. The right graph, Fig. 5(b), depicts the suggested reaction mechanism according to their DEMS study. At a temperature of $T = 90\,^{\circ}C$ and a catalyst Pt/C loading of 8 mg cm^{-2} 86% of the supplied 0.1 M EtOH were eventually oxidized to CO_2. Acetic acid was identified as a dead end which could not be further oxidized when it was supplied as anolyte to the MEA, as also reported by another study [42].

A MEA operating at intermediate temperatures (235–260 °C) was presented by Shimada et al. [26]. The EOR was studied on carbon-supported platinum catalyst (2 mg cm^{-2}) and CsH_2PO_4 served as proton conducting solid electrolyte. The C—C bond dissociation ratio was reported to be as high as 90% at 250 °C, almost independent of the applied potential, while the CCE reached more than 80% even with a water/ethanol molar ratio of 3:1. Other products were CH_4 and an almost negligible amount of AAL. H_2 was produced and oxidized in parallel to ethanol oxidation. As CH_4 formation reduces the CO_2 yield it is necessary to suppress this reaction pathway by an accelerated OH formation.

2.2. Ethanol oxidation reaction in alkaline media

Tripković et al. found that the kinetics of methanol oxidation on Pt and PtRu are one order of magnitude higher in alkaline media than in acid solutions [25]. This is mainly attributed to the increased adsorption of OH_{ads} which can help to oxidize the adsorbed CO_{ads}. As this oxygen containing group is also of great importance for the EOR [20,39,40,43], enhanced kinetics are expected for the anode reaction of alkaline direct ethanol fuel cells (ADEFCs). This notion is backed up by density functional theory (DFT)-studies that indicate that oxidation of ethanol is pH dependent because of its sensitivity to the amount of adsorbed OH [44].

Similar to the EOR in acid media the oxidation of ethanol in alkaline media was studied by electrochemical methods [45,46] or electrochemistry in combination with FTIR [47,48], DEMS [41,49,50] or chromatography [51,52].

Eq. (6) gives the full oxidation of ethanol to CO_2 in alkaline media:

$$CH_3CH_2OH + 12OH^- \rightarrow 2CO_2 + 9H_2O + 12e^- \quad (6)$$

The challenge remains to fully oxidize the ethanol which releases 12 electrons and not to end up with AAL or AA (or rather the acetate ion), because both diminish the faradaic efficiency [52]. Table 3 lists work performed to determine the products of ethanol oxidation in alkaline media under various parameters.

The reaction scheme proposed in most studies listed in Table 3 resembles the one shown in Fig. 5(b). AAL is seen as an active reaction intermediate that can be oxidized further while acetic acid (acetate ion) is thought to be a final product [45,46,52]. Among the listed publications two DEFC setups show the highest CO_2 yield [41,52]. For their measurements under fuel cell conditions Shen et al. named the operating temperature as the most important parameter to influence CO_2 selectivity [52]. While increasing the temperature from 60 to 100 °C they simultaneously observed an increase in the CCE from 6.0% to 30.6% on a Pd/C anode. Fujiwara et al. attributed their lower findings for the CO_2 yield (see Table 3), as compared to the work of Rao et al. [41], to a lower temperature (25 °C compared to 60 °C) and a lower potential (0.5 V vs. RHE compared to 0.8 V vs. RHE) [46]. Whether the higher potential significantly attributes to the found difference in selectivity for CO_2

Table 2
Overview about some publications dealing with the EOR of ethanol in acidic media. When there are multiple parameters given for one CO_2 yield then the parameters for which that specific value was obtained are printed in bold format. AA is acetic acid, AAL is acetaldehyde and EtOH is ethanol. CCE stands for CO_2 current efficiency.

Setup	Conc. EtOH	Temp (°C)	Catalyst	Spectroscopy	Main product	CO_2 yield	Remarks	Source
DEFC	H_2O:EtOH 2:1–**5:1**	150–190	PtRu, **Pt-black**	MS	AAL	40%	Results independent of temperature in inv. range.	[29]
3-Electrode cell	5 mM–0.2 M	10	Polyc. Pt	FTIR	AAL, AA	n.a.	AA dominant at low EtOH conc., AAL at conc. > 0.1 M.	[22]
DEFC	1.0 M	145	PtRu/C, Pt	GC	CO_2	>95%	Cell pressurized (anode at 4 atm, cathode at 5.5 atm).	[36]
3-Electrode cell	1.0 M	5–40	$Pt_xRu_{(1-x)}$, $(1.0 < x < 0.5)$	DEMS	CO_2	n.a.	Highest selectivity at $x = 0.85$ and $T = 40$ °C.	[30]
3-Electrode cell	**0.01**–1 M	25	Polyc. Pt	FTIR	AA, AAL	~10%	Above 0.1 M EtOH, AA and CO_2 generation inhibited.	[34]
3-Electrode cell	**0.001**–0.01–0.5 M	23–30-60	**Pt/Vulcan**, polyc. Pt	DEMS	AAL, AA	7.5%	AA dominant at low EtOH conc., AAL at conc. > 0.5 M.	[29]
Thin layer flow cell	0.01, 0.1 M	23	Pt/Vulcan, Pt_3Sn/Vulcan, PtRu/Vulcan	DEMS	AA	1%	Addition of Ru or Sn lowers onset potential for EOR, selectivity not increased.	[28]
3-Electrode cell, DEFC	0.1 M	50–110	Pt/C, PtRu/C, PtSn(9:1)/C,	In situ IR reflec.	AA, AAL	n.a.	For tin modification CO adsorbs easier, dissociation of EtOH is faster.	[35]
DEFC	2.0 M	80	**Pt/C**, PtSn/C, PtSnRu/C	HPLC	AA	20%	Addition of Ru or Sn lowers onset potential for EOR, selectivity not increased	[37]
DEFC	0.01, **0.1**, 1.0 M	30, 60, **90**	**Pt/C**, PtRu/C, PtSn(7:3)/C	DEMS	CO_2	86%	AAL can be further oxidized to CO_2, AA not.	[24]
DEFC	1.0 M	90	PtSn/C, PtRu/C	GC	AA	n.a.	Catalytic activity toward AA higher for PtSn/C than for PtRu/C.	[23]
DEFC	H_2O:EtOH 3:1	235–260	Pt/C	GC	CO_2, H_2, CH_4	CCE ~ 80%	C—C bond dissociation > 90%.	[26]

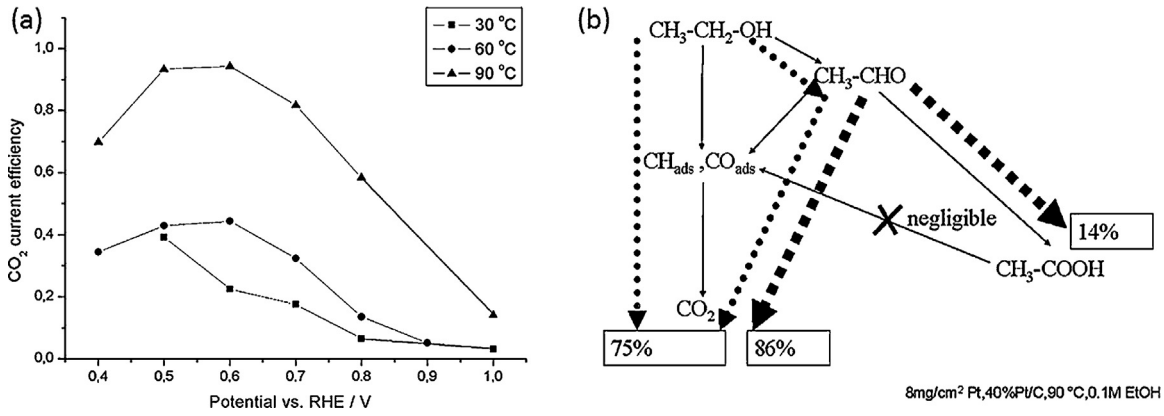

Fig. 5. (a) CCE over Potential vs. RHE at the anode of a membrane electrode assembly featuring a metal loading of 5 mg cm^{-2} of Pt/C at different temperatures. The concentration of ethanol was 0.1 M. (b) Scheme of Ethanol oxidation in fuel cell conditions.
Reprinted with permission from [41], Copyright 2007, The Electrochemical Society.

oxidation is dubious however, as CO_2 is mainly generated from CO_{ads} which is formed by associative adsorption of ethanol at low potentials [52]. Bayer et al. claimed that CO_2 can only be formed from adsorbed ethanol and not through bulk oxidation [50]. Interpreting results obtained from stripping voltammetry with coupled DEMS on a Pt electrode, it was proposed that ethanol adsorbs at potentials between 0.2 and 0.4 V vs. RHE. It can be oxidized to CO_2 from CO_{ads} at potentials lower than 0.9 V vs. RHE and from CH_x or CO_xH_y at potentials higher than 0.9 V vs. RHE, although potentials higher than 0.4 V vs. RHE are not relevant for fuel cell operation [53].

By investigating the EOR on a Pd electrode in various concentrations of NaOH the dependence of ethanol electro-oxidation on the pH value was determined [47]. While the highest current densities were detected in 1 M NaOH, CO_2 evolution was only detected below pH 13. These findings stress the significance of large amounts of OH_{ads} to achieve high oxidation activity. However, abundance of OH_{ads} seems to impede ethanol adsorption which is prejudicial to CO_2 formation.

2.3. Intermediate temperature direct ethanol fuel cells membranes

There is some agreement within the DEFC community that in order to accelerate the kinetics of the EOR, thus to make lower precious metal catalyst loads and higher EtOH concentration feasible, the temperature of the fuel cell needs to be increased [26,31,35,37,46,51,54,55]. This requires an electrolyte suitable for these temperatures. Mechanical, thermal and cycle stability as well as high ionic conductivity have to be met by the membrane material.

Perfluorosulfonic membranes of the Nafion® type are usually considered as first choice for PEMFCs. They are not suitable for a DEFC working at intermediate temperatures, however, because they release water at temperatures higher than 373 K, which deteriorates their conductivity, and the glass transition temperature lies around 403 K [56].

Modifications of Nafion® membranes with metal oxides MO_2 (M = Zr, Si, Ti) improve their thermo-mechanical stability. Nafion®-ZrO_2 outperforms unmodified Nafion®-membranes in terms of water uptake and conductivity, but this modification can raise the maximum operation temperature only to 393 K [57].

Other oxygen ion and proton conductors which do not contain water and can operate in the intermediate temperature range 400–800 K for FC applications are still in a development stage [58]. Proton conductors made either from salts of inorganic oxygen acids [59] or inorganic materials without water [60] as well as ionic lattice conduction of oxide ceramics suitable for operation at 773 K [61,62] were intensively investigated.

As shown in Table 2 and reported in Section 2.1, Shimada et al. presented a DEFC working in a temperature range of 508–533 K [26]. They employed a CsH_2PO_4/SiO_2 (SiO_2: 1 wt.%) electrolyte to prepare their MEA. CsH_2PO_4 is a hydrogen-bonded oxyacid proton conductor which exhibits a reversible phase transition at T_c = 503 K [63,64]. The high temperature cubic phase is stable and shows a high conductivity of >10^{-2} S cm^{-1} under appropriate humidity conditions [63]. Added SiO_2 enhances conductivity due to its hydrophilicity and the introduction of point defects. However, it seems as if the high conductivity of CsH_2PO_4 can only be maintained in the relatively narrow temperature range from 508 to 533 K, requiring high pressure or humidity [65].

Another possible candidate for a membrane material for intermediate DEFCs is ammonium polyphosphate (NH_4PO_3) [65–68]. When a framework material is added the melting point can be increased and the conductivity is high [66]. Haufe et al. studied the polyphosphate composite $[NH_4PO_3]_6[(NH_4)_2SiP_4O_{13}]$ by chemical analysis, X-ray diffraction, thermal gravimetry, impedance spectroscopy and NMR techniques at temperatures up to 573 K [67]. They found that the material is stable after an initial weight loss due to ammonia release and showcases a high conductivity of 0.1 S cm^{-1}, as it can be seen in Fig. 6. Matsui et al. from the Kyoto University also reported high conductivities for the composites $[NH_4PO_3]_6[(NH_4)_2MP_4O_{13}]$ (M = Ti and Si) with activation energies as low as 0.39 eV and 0.21 eV, respectively, in ambient air [69,70]. They reported structural changes at intermediate temperatures which resulted in peculiar ionic-conducting properties and could not assign the observed effect to either the matrix or the decomposed species. This was later clearly answered by Wang et al. who investigated a series of six composites with the structure $[NH_4PO_3]_6[(NH_4)_2Si_{1-x}Ti_xP_4O_{13}]$ ($0 \le x \le 1$) and concluded that the contribution of the metal cations to the transport properties is minor [71]. Once more, they confirmed high conductivities in a temperature range of 400–550 K.

In general, it was shown that the ammonium polyphosphate materials could prove to be a good candidate for intermediate temperature FCs as they feature high conductivity in the desired temperature range (423–473 K) [72,73]. This is associated with small activation energies providing sufficient conductivity down to room temperature. Recently, the preparation of a flexible membrane was achieved making the fabrication of a MEA

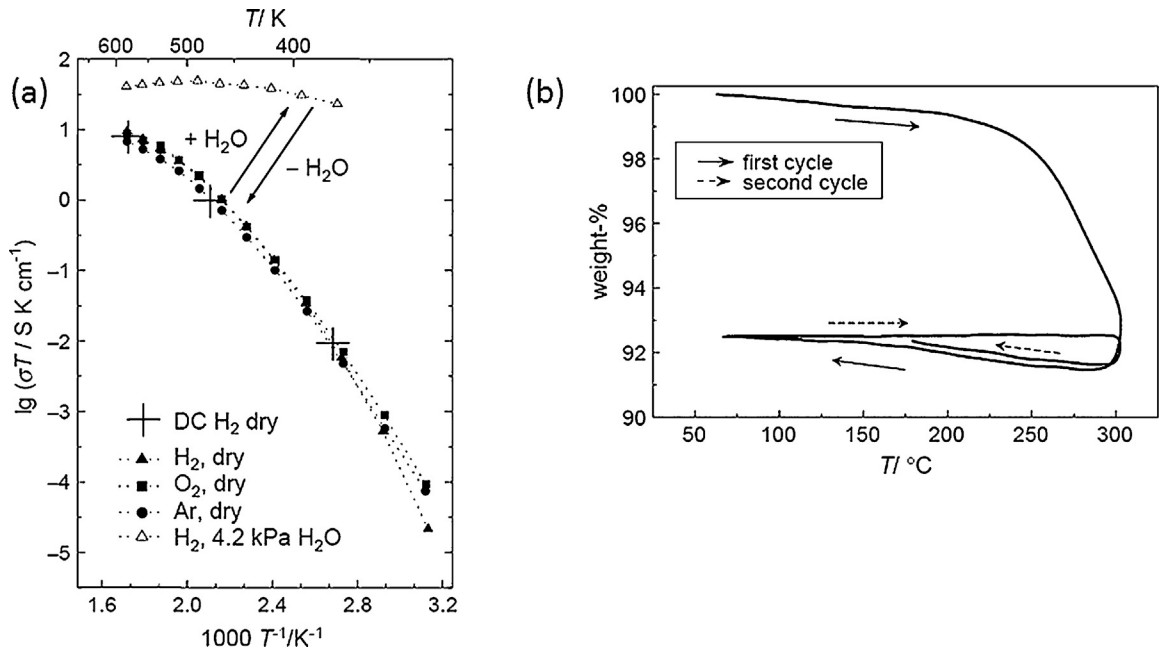

Fig. 6. (a) Arrhenius plot of conductivity σT determined in various atmospheres by AC conductivity measurements. Only three values, denoted by +, are determined by DC measurements in a H_2—H_2— cell. (b) Mass loss of $[NH_4PO_3]_6[(NH_4)_2SiP_4O_{13}]$ at a heating rate of 10 K/min in a dry H_2 atmosphere.
Reprinted from [67], Copyright 2005, with permission from Elsevier.

more straightforward [74]. Future work should be aimed at either improving mechanical stability or at gaining a deeper understanding of the adsorption/desorption process of water which is correlated with the mechanism of ion transport.

A review on the status of alkaline anion-exchange membranes (AAEMs) for alkaline fuel cells [75] or reviews on alkaline fuel cells with a section dedicated to AAEMs [76,77] were published recently. It is stated that besides considerable efforts commercial AEMs are in an early stage of development. Key issues are to explain the transport mechanism of hydroxide anions and to increase the conductivity [75]. Another constraint is the precipitation of carbonates from the CO_2 generated at the anode on the electrode which can destroy the active layer [77,78].

3. Model catalyst research

As shown in Tables 2 and 3 much work was performed in order to investigate the reaction pathways of the EOR on various electrodes. Polycrystalline platinum and compounds of platinum with admixtures of other metals such as tin, ruthenium or rhodium supported on carbon materials served as electrodes.

However, ultimate goal of catalyst research is to design and tune the activity of catalysts by careful control of their compositional and structural properties, down to the level of atoms. This would lay the foundation for an 'atomistic engineering' of surfaces [79]. The activity toward a certain reaction is a measure for how well the catalyst promotes the process by enabling the four single functions of a catalyst: Firstly, the catalyst adsorbs the target molecule and cleaves its bonds. It then keeps the reactants at close proximity to the boundary surface. By definition, the catalyst facilitates the targeted reaction or even enables new pathways. And lastly, when the desired reaction took place, the catalyst has to release the products so that the catalyst site can become active again.

The exchange current density j_0 is a good measure for the electrocatalytic activity. Fig. 7 shows an example of the Volcano plot for the HOR/HER, giving $\log(j_0)$ vs. the free adsorption energy ΔG_{H^*} of hydrogen on the respective metal [80]. It can be seen as pivotal achievement of catalyst research. Based on work which started as early as the 1950s [81,82], theoretical and experimental research culminated in the understanding of the trends and that the maximal rate for HOR and HER can be achieved when $\Delta G_{H^*} \approx 0$ [83–85].

As real catalyst systems are rather complex one has to develop a model to correlate the different parameters. These parameters are, besides the composition of the supported nanoparticles, their size [87–89], their dispersion [90,91], the coordination of surface atoms [92–94] and the influence of the substrate material [95–99]. Enhanced mass transport due to spherical diffusion toward 0D particles also has to be considered [100–102].

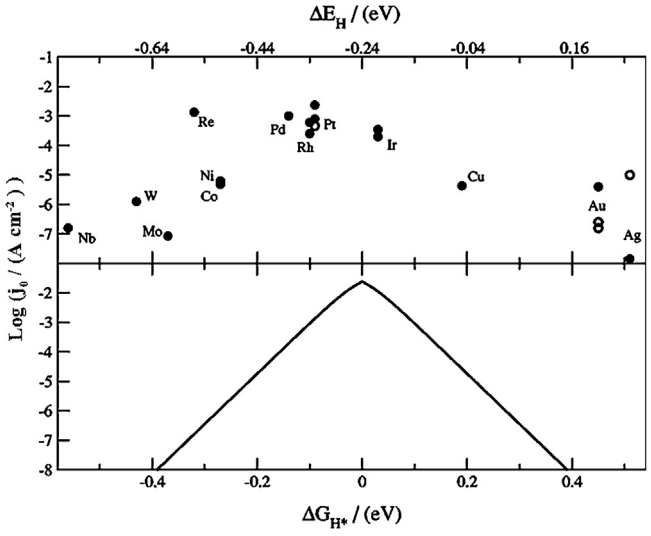

Fig. 7. Top part shows experimentally measured exchange current densities for HER/HOR as a function of calculated hydrogen chemisorption energy per atom, ΔE_H. Bottom part shows a simple kinetic model plotted as a function of the free energy for hydrogen adsorption ΔG_{H^*}. $\Delta G_{H^*} = \Delta E_H + 0.24$ eV.
Reproduced with permission from [86], Copyright 2005, The Electrochemical Society.

Table 3
Overview about some publications dealing with the EOR of ethanol in alkaline media. When there are multiple parameters given for one CO_2 yield then the parameters for which that specific value was obtained are printed in bold format. AA is acetic acid and AAL is Acetaldehyde. CCE stands for CO_2 current efficiency.

Setup	Conc. EtOH	Temp (°C)	Catalyst	Spectroscopy	Main product	CO_2 yield	Remarks	Source
DEFC	1.0 M	25	PtRu: 3 mg cm^{-2}	Enzymatic analysis	AA (92%)	~7%	Results for 30 mA cm^{-2} at 0.28 V vs. RHE	[46]
3-Electrode cell	1 M	Not given	Pd	FTIR	AA	Not given	CO_2 formation only for pH < 13	[47]
3-Electrode cell	0.1 M	Not given	**Polycryst. Pd**, polycryst. Pt, Pd black	FTIR	AA	<2.5%	0.1 M NaOH, C—C bond breaking capability of Pd slightly higher than Pt.	[48]
Thin layer flow cell	**0.01 M**, 0.1 M	Not given	**Pt**, Pd, Au, Ni	DEMS	AA	<5%	Current eff. for AA highest on Pd, for CO_2 highest on Pt	[49]
Thin layer flow Cell	**0.01 M**, 1 M	22	Sputtered Pt	DEMS	AAL	CCE 20%	CCE > 10% only below 0.6 V vs. RHE (CO_{ads} oxidation)	[50]
3-Electrode cell	1 M	Not given	Pt, Pd	HPLC	AA	Not detected	Pd and Pt current densities similar	[51]
DEFC	**0.2 M**, 0.5 M, 1 M	60–**100**	**Pd/C**: 1 mg cm^{-2}, Pd_2Ni_3/C	Gas and ion. chrom.	AA	CCE 31%	Operating temperature most important parameter	[52]
DEFC	0.1 M	60	Pt	DEMS	CO_2	CCE 55%	Same setup in acid showed only 2% CCE	[41]

3.1. Creating nanostructured model surfaces

Well defined electrode surfaces are of utmost importance for the understanding of reactions at interfaces. Therefore, mostly single crystals or highly oriented pyrolytic graphite (HOPG), which is a sp-2 hybridized carbon and shows a very high degree of three-dimensional ordering, are employed either as electrode themselves or as support for dispersed particles [103–106].

For single crystals the orientation of the crystal face can influence the kinetics. Marković et al. showed that the exchange current density of the HER increases in the order Pt(1 1 1) < Pt(1 0 0) < Pt(1 1 0) for platinum low-index single crystal surfaces. They attribute this effect to structure-sensitive heats of adsorption of the reaction intermediate H_{ads} [103,107,108]. Fig. 8 shows results from these investigations. Similar studies were for example performed for gold [109], palladium [110–113] or ruthenium [114,115].

As support for foreign metals especially Au(1 1 1), HOPG and, to some extent, Ru are important. These materials are quite inert and show a low activity themselves [116]. HOPG is often used as carbon support model due to its high overpotentials for HOR and HER and because its surface is an almost smooth graphite basal plane [105,106,117].

Second step in the creation of a model catalyst system, after creating a suitable surface, is deposition of single particles or small clusters onto the substrate. Besides others [118–120], two possible ways to form nanostructured modifications are electrochemical metal deposition or top-down lithography methods.

Kolb and Simeone reviewed different methods how nanolithography can be performed by either a scanning tunneling microscope (STM) or a electrochemical scanning tunneling microscope (EC-STM) [121,122]. Techniques which can be performed by a STM tip are for example the creation of nucleation centers by mechanical interaction between tip and substrate [123,124] or the local removal of a tarnishing film with the tip which makes metal deposition at the freshly uncovered sites possible [125]. Conceptually different is the so-called jump-to-contact method [126–128]. As laid out in [129], metal ions from the solution are deposited on the tip. Upon successful loading the tip is brought so close to the surface that the jump-to-contact occurs which leads to the formation of a metal bridge, the connective neck, between substrate and tip. A successive retreat of the tip leaves a small metal cluster on the surface. Main advantages of this method are that it can be performed at kHz rates, the STM tip can 'read' the produced pattern after 'writing' it and that the cluster size can be varied within certain range [122].

Electrochemical metal deposition is a fast and convenient way to decorate surfaces with a well-defined amount of foreign metals from solution [106]. While the actual mechanism of the particle growth is still subject of scientific debate [130,131], electrodeposition is an important method to synthesize supported nanoparticles. It was shown that pulse deposition can form a relatively uniform distribution of particles, for example Pt on HOPG [132]. However, the deposition reaction may run into mass-transport limitation when high overpotentials are applied or particles are in close proximity on the surface. As the depletion zones overlap more for particles with close and many neighbors they grow slower and therefore single pulses lead to increasing size dispersion [133,134]. This diffusional coupling effect can be mitigated by applying a short (≈ms), high-overpotential nucleation pulse followed by a low-overpotential growth pulse. The longer (≈100 s), second pulse leads to steady growth of metal particles without further nucleation [135,136]. Recently Brülle et al. demonstrated that using the double-pulse technique they can tune the size of platinum particles on a boron-doped diamond (1 0 0)-surface between 1 and 15 nm in height and 5 and 50 nm in apparent radius while keeping the particle density constant [137].

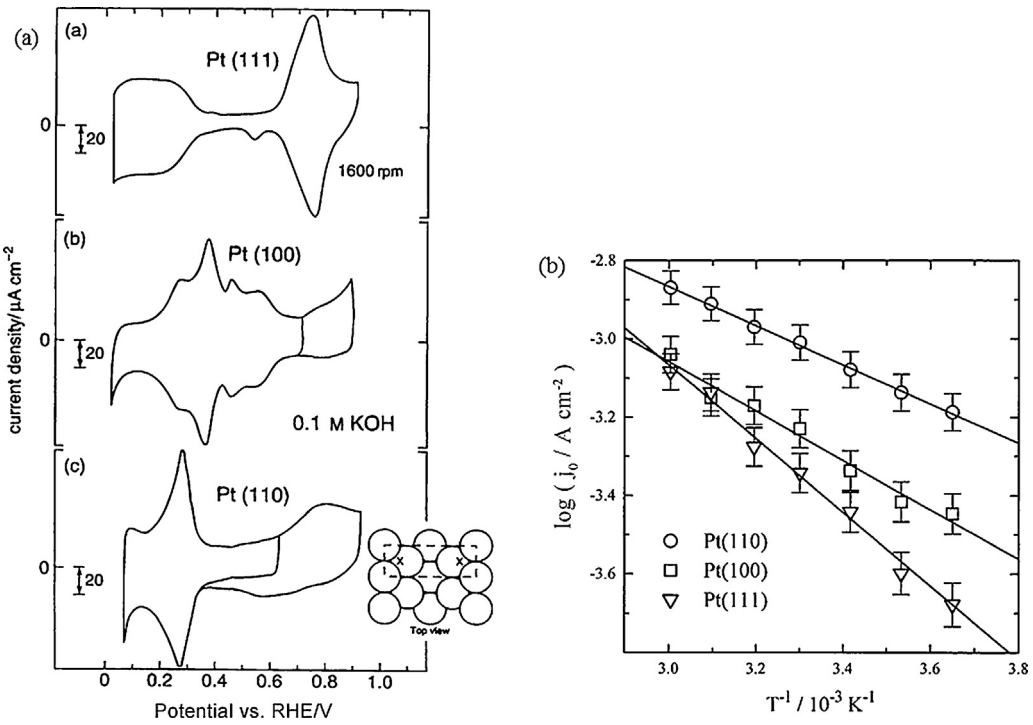

Fig. 8. (a) Cyclic voltammograms on a Pt($h\,k\,l$) rotating disk electrode (RDE) in oxygen-free 0.1 M KOH. The disk was rotated at 1600 rpm while employing a potential sweep with a rate of 50 mV/s. Reproduced from [103] with permission from The Royal Society of Chemistry. (b) Arrhenius plots of exchange current densities j_0 for Pt($h\,k\,l$). Electrodes were immersed in a 0.05 M H_2SO_4 solution. Reproduced from [108] with permission from the American Chemical Society.

3.2. Reactivity measurements

Creating a suitable nanostructured model system is the first step which needs to be performed in order to experimentally identify parameters which influence reactivity. Second and third step are to measure the reactivity of created nanostructures and to combine these findings, often assisted by theoretical calculations and models, to a valid theory.

Such a holistic approach was demonstrated by a joint project of the Technical Universities Denmark and Munich [138]. They investigated the catalytic activity of single palladium particles on a gold surface toward the HER. To resolve the influence of every single layer of Pd on the substrate they employed an STM tip for the proton reduction reactivity measurement. Fig. 9(a) shows the working principle of this method and details can be found in ref. [139]. It was shown that a decrease in particle height from 200 nm to 6 nm enhances the reactivity by more than two orders of magnitude, while it approaches the theoretical value for bulk Pd(1 1 1) at a thickness of roughly ten monolayers. Using calculations and molecular dynamics simulations these results, as presented in Fig. 9(b), could be explained by the support induced strain [138]. The Au(1 1 1) substrate causes an expansion of the Pd lattice which in turn shifts up the electrode d-band and leads to an increased overlap with the orbitals of the adsorbed hydrogen [113,140,141].

This work points toward an important method for a systematic engineering of nano-catalysts, as lattice mismatch leads to a variation of surface strain for different particles sizes. This in turn changes activation energies and adsorption energies not only for hydrogen but for other relevant molecules too [142]. What differentiates this work from other work on the catalytic activity of Pd layers on Au(1 1 1), like [110,112], is the fact, that the high local resolution of the STM tip makes sure that the actual observable is not the average activity of multiple particles with different thicknesses caused by the size distribution of deposited materials.

In our group the influence of palladium coverage on Au(1 1 1) on the specific reactivity of the HER [84,143] and the HOR [144] was investigated in the range of sub-monolayers to several monolayers. For coverages larger than one monolayer a behavior similar to the one discussed in [138] was found, however, with a much smaller dependence on the number of Pd layer.

Decreasing the amount of deposited Pd to sub-monolayers leads to a further increase (Fig. 10). This cannot be explained by the lattice distortion.

A possible explanation is spillover of reaction-intermediates. During this effect, described by Eikerling et al. for the HER [145], hydrated protons diffuse from the bulk onto the Pd islands on which they are reduced and form strongly adsorbed atomic hydrogen H_{ads}. The generated H_{ads} diffuses on the particle and spills over to the surrounding Au-substrate. There recombination of adsorbed atomic to adsorbed molecular hydrogen ($2H_{ads} \rightarrow H_{2,ads}$) takes place. Finally the $H_{2,ads}$ desorbs, forming molecular hydrogen. As this mechanism frees active sites on the catalyst particle it accelerates the fourth function of a catalyst, release of generated product, increasing the rate at which hydrogen is formed. A spillover may not be favorable from an energetic point of view when looking at Pd particles with low ($\theta \ll 1$) H_{ads} coverage [146], but for hydrogen evolution the coverage is θ close to 1. This direct influence of the Au(1 1 1) support can also be responsible for increased rates of the HOR [116].

Löffler et al. suggest that step-sites increase catalytic activity [147], but no significant dependence of the current density on the number of terrace atoms was found by either Pandelov et al. [84] or by single particle measurements [138].

Enhanced mass-transport due to hemispherical diffusion toward small catalyst islands [100–102] is another explanation but cannot be the sole reason as lower currents were measured in a similar experiment with Pt sub-monolayers on HOPG [137] and the type of diffusion should be independent on the substrate.

A combination of these three reasons is the most probable explanation for the enhanced activity of sub-monolayers. The effect is so

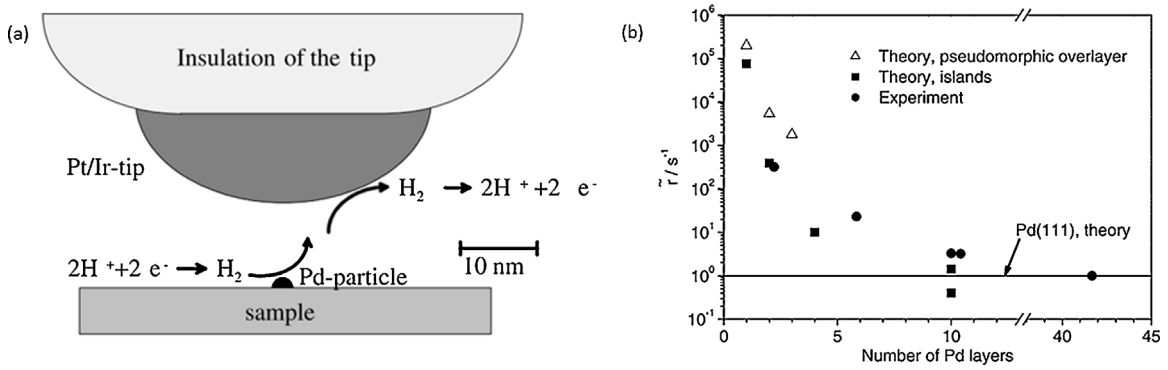

Fig. 9. (a) Illustration of single particle reactivity measurement with a STM-tip. The particle was also created with the STM-tip (see [126]). (b) Semi-logarithmic plot showing the relative reaction rate vs. number of Pd layers. Full circles were experimentally obtained, open triangles are calculated using DFT for pseudomorphic layers. Full squares represent theoretical predictions for islands obtained from a combination of DFT and molecular dynamics.
Reprinted from [138], Copyright 2004, with permission from Elsevier.

strong that even the current density per geometric area increases with decreasing coverage of Pd.

Wolfschmidt et al. also investigated the HER, HOR and oxygen reduction reaction (ORR) for mono-atomic layers of Pt on Au(1 1 1) [100]. While the ORR shows a decrease in reactivity with decreasing amounts of deposited Pt, HOR and HER feature a strong increase in specific activity when the coverage θ is smaller than 1.

Refining these experiments specific exchange current densities per Pt-surface from hydrogen related reactions as high as several 100 mA cm^{-2} for coverages below 0.0025 monolayers platinum on Au(1 1 1) were reported [100]. For single Pt particles the specific exchange current densities are even higher, several A cm^{-2} to several 10 A cm^{-2}, depending on the number of atomic layers (AL) of the particle. These results can be seen in Fig. 11.

Similar values in the order of 1 A cm^{-2} were also reported by Gasteiger and co-workers [90,91]. Comparison of these values with the maximum specific exchange current densities given in the volcano plot, see Fig. 7 and Refs. [83,86], indicates that either some effects of nano-structured surfaces need to be implemented in a revised volcano-model or too low current densities were measured in the past [100]. Since structural effects can increase the specific activity of catalyst surfaces by orders of magnitude, an expansion of the volcano plot by another dimension, to incorporate such effects, might have to be considered.

Further studies clearly showed that these high observed current densities are correlated with the choice of substrate. When depositing platinum nanoparticles on HOPG [106] or highly boron-doped and 1 0 0-oriented epitaxial diamond [137], no influence of the particle size or the coverage on the activity for HER and HOR was observed. The obtained values were always close to the exchange current densities for bulk platinum.

4. Model catalyst research for the ethanol oxidation reaction

Model catalyst research encompasses investigations which make use of carefully designed structures in order to investigate the influence of one single parameter such as particle size, support material, catalyst dispersion, coordination surface atoms or influences of mass transport, as discussed earlier. It is of utmost importance to keep the multidimensional parameter space influencing the activity constant except for the one observable under investigation to test a specific hypothesis.

In the following, we will review the status of model catalyst research performed for the EOR, both in acidic and alkaline media. We will elaborate on the influence of coordination, composition, substrate, particle size and dispersion, provided that there are reports in the literature. As it is of significance for the EOR we will

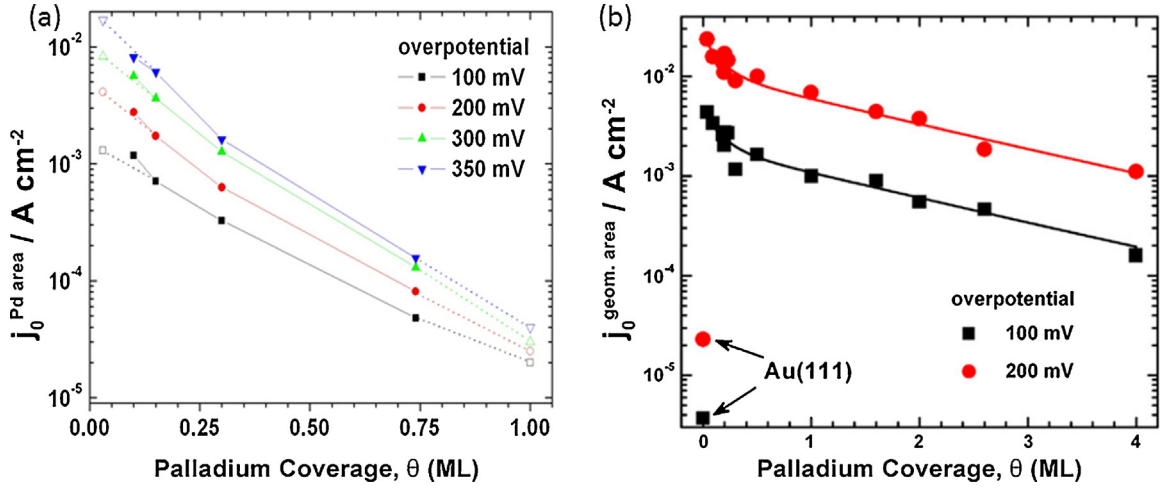

Fig. 10. (a) Exchange current density normalized to Palladium area $j_0^{\mathrm{Pd\,area}}$ over Pd coverage θ as fraction of one monolayer (ML) for the HOR. Potentiostatic pulses were employed to obtain data points. Reprinted with permission from [144]. (b) Exchange current density normalized to geometrical electrode area $j_0^{\mathrm{geom.\,area}}$ over palladium coverage θ for some MLs for the HER. Galvanostatic pulses were employed to obtain data points. Reprinted from [84], Copyright 2007, with permission from Elsevier.

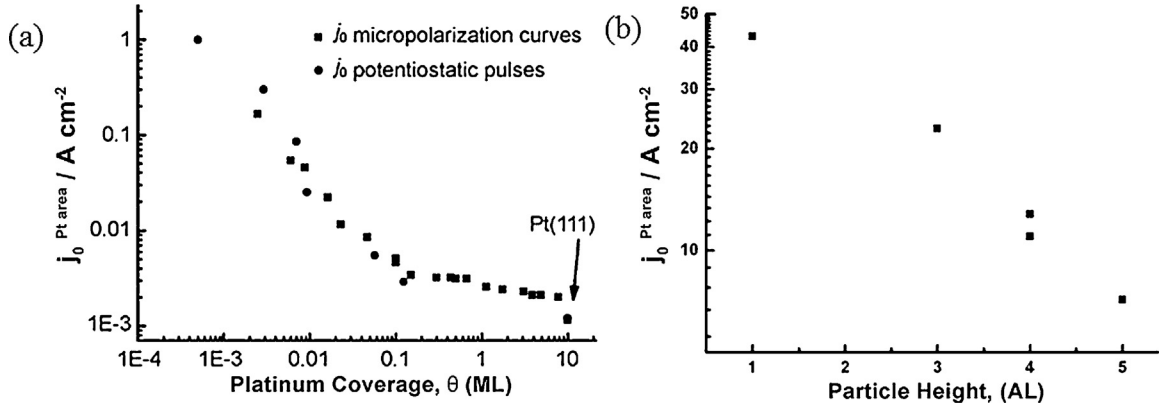

Fig. 11. Exchange current density normalized to Platinum area $j_0^{Pt\,area}$ for hydrogen reactions vs (a) Pt coverage θ given in monolayers on Au(1 1 1) and (b) particle height of single Pt paprticles on Au(1 1 1) given as mulitples of an atomic layer (AL).
Reprinted with permission from [100], Copyright 2010, John Wiley and Sons.

treat the degree of alloying of bi-metallic catalysts as an additional parameter. In addition, we will discuss experiments dealing with temperature dependence of some catalysts for the EOR.

4.1. Acid media

Starting from non-poisoned Pt(1 1 1), Pt(1 1 0) and Pt(1 0 0) electrode surfaces the adsorption of CO_{ads} and evolution of CO_2 was monitored with FTIR while applying potentials steps in 0.1 M or 1 M EtOH solution in a flow cell [148]. Correlation of these spectra with CV data of the three Pt basal planes allows drawing conclusions toward potential dependence of CO_{ads} coverage and capability of the planes to cleave the C—C bond. Pt(1 1 1) not only shows the lowest intensity of CO_{ads}, it also exhibits the lowest activity toward C—C bond splitting. Both the Pt(1 0 0) and the Pt(1 1 0) basal plane are more active for C—C bond cleavage than Pt(1 1 1), which one of the two shows the highest activity could not explicitly be answered by the authors. Also, when comparing the C—C splitting rate on Pt(1 1 1) with polycrystalline and stepped (Pt(3 5 5)) platinum, the Pt(1 1 1) basal plane shows a lower activity, producing less CO_2 [149].

Colmati et al. confirmed that on Pt(1 1 1) mostly AA is formed as it shows little or no CO_{ads} coverage [150]. They were able to detect a difference in activity for Pt(1 0 0) and Pt(1 1 0), and assigned the higher C—C splitting activity to the Pt(1 1 0) electrode. Looking at (1 1 0) and (1 0 0) steps on Pt(1 1 1) terraces Colmati et al. further refined the understanding of the influence of the different crystal planes [151]. Following the trends for basal planes [148,150], Pt(1 1 0) steps are very active for C—C splitting. To enable the oxidation of CO_{ads}, however, an adsorbed OH_{ads} species is required [20,39,40], which is not readily supplied when the entire surface is covered with CO_{ads}. Therefore, an intermediate C—C cleavage rate, as obtained for the Pt(5 5 4) surface, combining Pt(1 1 1) with Pt(1 1 0) properties, is found to produce optimal catalytic conditions. The same trend was reported by Lai and Koper when investigating terraces larger than 10 atoms [152]. Fig. 12 shows the maximum current density and the peak potential vs. RHE of bulk ethanol oxidation on Pt(1 1 1), Pt(15 15 14), Pt(5 5 4), Pt(5 5 3) and Pt(1 1 0) electrodes in H_2SO_4 and $HClO_4$. The highest current densities were achieved on Pt(5 5 4) in $HClO_4$ and on Pt(5 5 3) in H_2SO_4. The influence of the supporting electrolyte can be explained by preferential adsorption of bi(sulfate) which takes place on terraces rather than on steps [152,153]. A first theoretical attempt to explain the reaction mechanism on different model catalyst surfaces was performed by Wang and Liu [154]. The authors employed DFT-studies to locate transition states and saddle points of the EOR on Pt(1 1 1), Pt(2 1 1) and Pt(1 0 0). In accordance with the experimental studies they calculated that the Pt(1 0 0) surface shows higher activity for total oxidation of EtOH than the two other surfaces under investigation. The surface sensitivity of the EOR was attributed to initial dehydrogenation of ethanol and oxidation of CH_3CO (see Ref. [20]). In order to facilitate those two reaction steps a high bonding ability of surface atoms with unsaturated C-containing fragments and high stability of OH_{ads} is required. Both properties are influenced by the surface coordination.

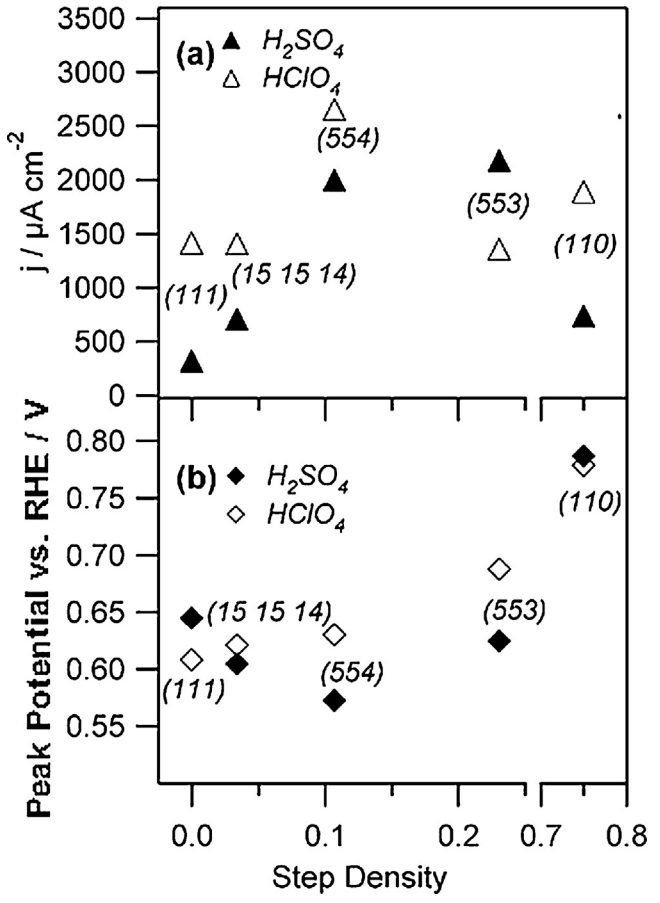

Fig. 12. (a) Maximum current density and (b) peak potential vs. RHE of bulk ethanol oxidation over step density in 0.5 M H_2SO_4 and 0.1 M $HClO_4$ on different Pt model electrodes.
Reprinted with permission from [152], Copyright, 2008, Royal Society of Chemistry.

Besides looking at the coordination of Pt another approach is to change the composition of the catalyst, combining the Pt with a second metal to obtain a binary catalyst. This can lead to an electronic effect, e.g. changes in the adsorption energy, on the one hand, and, on the other hand, allows for a bi-functional mechanism [155]. Examples for added metals are Ru, Ni, Mo or Sn [156].

The reasoning behind this bi-functional mechanism is similar to the superiority of Pt(5 5 4) over Pt(1 1 0), although the latter is more active toward C—C bond cleavage [151,152]. Pt by itself shows the highest activity for the C—C bond cleavage. High coverage of CO_{ads} on platinum, however, blocks sites for OH_{ads}, which impedes the oxidation to CO_2 [32]. The required surface oxygen groups can be supplied by the adjacent co-catalyst atom, allowing for higher activity [55].

Tsiakaras investigated the influence of additions of Ru, Pd, W and Sn on the platinum lattice parameter [55]. While addition Ru or Pd decreases the lattice parameter it is increased by Sn or W. The activity of the prepared binary catalysts for the EOR increased in the order PtPd < PtW < PtRu < PtSn and to further investigate the best catalyst, ratios ranging from Pt_1Sn_1 to Pt_4Sn_1 were prepared. This resulted in an almost volcano-formed shape, when plotting peak power of a DEFC with the respective catalysts over atomic percentage of Sn. The apex of the volcano forms due to interplay of enhanced activity with expanding lattice and decreased conductivity with higher amounts of semiconducting tin oxide [157]. The optimal Sn content for temperatures from 60 to 90 °C was found to be 30–40% [55]. A slightly higher value of 50% was reported by Kim et al. for EOR at room temperature, showing a similar volcano plot [158]. It was alleged that the operating temperature has an influence on the optimal composition [155]. The increase in lattice parameter might lead to an electronic effect, shifting the d-band of the Pt down, as reported for Pt_3Sn [159,160].

The oxidation state of the Sn in the bimetallic catalyst, whether it is alloyed as PtSn or in the oxide form $PtSnO_x$, has been reported to be of importance for the reaction mechanism [161–163]. Godoi et al. were able to investigate the activity of $PtSnO_x$ catalysts with different amounts of alloyed and oxidized forms of Sn while keeping the same overall composition (Pt:Sn = 7:3, particle size ≈ 3 nm) [161]. The obtained ethanol oxidation currents were higher for catalysts which were treated in hydrogen atmosphere and therefore showed a higher degree of alloying than for catalysts with a higher amount of oxidized Sn. The authors assign this enhancement to an electronic effect which is caused by increased filling of the Pt 5d band when the amount of alloy increases.

Antolini and Gonzalez reviewed the current status of PtSn catalysts for EOR, the effect of synthesis method and structural characteristics recently [155].

Besides the catalyst itself also the support might play a crucial role, as exemplified by the HER spill-over effect [100,145]. Multi-walled carbon nanotubes (MWCNTs) were compared to commercial Vulcan as support for PtSn catalyst [164]. CO stripping voltammograms and electrochemical impedance spectroscopy indicate higher exchange currents on the MWCNT support. However, as the authors do not factor in the increased surface area of the MWCNTs to normalize their results, it remains dubious if they really observe an effect caused by superior qualitative properties of the MWCNT support. They hypothesize that the higher observed currents are due to oxygenated surface functional groups acting as nuclei to anchor the PtSn particles, the improved electronic conductivity of the MWCNTs and improved metal-support interaction. In a similar fashion Pt and PtRu nanoparticles were investigated on graphene support and compared to graphite and Vulcan substrate [165]. While higher activity was asserted to catalysts on graphene, the actual surface area was not considered in that study.

While well-defined substrates like HOPG were employed for studies on the deposition of DEFC relevant catalysts like PtSn [166], there are few reports of the influence of model substrates on the EOR. One such work was performed by El-Shafei and Eiswirth [167]. They deposited Sn submonolayers on Pt(1 0 0), Pt(1 1 0) and Pt(1 1 1) single crystal electrodes and investigated what coverage of Sn shows the highest rate of EOR. For all the three investigated basal planes the addition of Sn enhanced the activity, the highest increase was found for Pt(1 1 0) on which it lead to a more than ten-fold increase in oxidation current. The optimum in coverage varied for different basal planes, they were 0.2, 0.25 and 0.52 of a monolayer for Pt(1 0 0), Pt(1 1 1) and Pt(1 1 0), respectively. Zheng et al. performed similar work and found that Sn adsorbs preferably on the hollow sites of the low-index basal planes Pt(1 1 1) and Pt(1 0 0). However, they were not able to achieve significant adsorption of Sn on Pt(1 1 0) single crystals [168].

Attempts to identify the influence of particle size were performed by comparing the activity of catalysts synthesized via the polyol-route with commercial ones, whereas the synthesized Pt/C, PtRu/C and Pt_3Sn/C catalysts particles were significantly smaller as compared to the commercial catalysts [169]. However, no size induced effects could be observed as a lower degree of alloy formation for the synthesized particles led to a decrease in activity which overlaid other effects (compare [161]). Another examination of Pt particles on carbon support for EOR in a half-cell revealed a maximum specific activity for a particle size of 2.5 nm. This was attributed to a compromise between structural effects and oxophilicity of the Pt surface [170].

4.2. Alkaline media

Due to challenges with the membrane material and carbonation which leads to membrane deactivation the EOR was much less studied in alkaline than in acidic media [171]. However, the activity for oxidation of organic molecules is higher in alkaline media as compared to acidic media [172].

Analogous to their work in acidic media [152] Lai and Koper investigated the EOR in alkaline media on Pt single crystal electrodes [171]. As it can be immediately seen in Fig. 13, which shows current over time transients for EtOH in $HClO_4$ (Fig. 13(a)) and NaOH (Fig. 13(b)), the initial current for the oxidation of ethanol is higher in alkaline media than it is in acid media. However, deactivation of the electrodes is more prominent in the alkaline solution and especially strong for surfaces with wide terraces, (Pt(1 1 1) and Pt(15 15 14)). This deactivation was related to $CH_{x,ads}$ species which cannot be stripped as easily as in acid media [152] and of which a higher amount was detected on Pt(1 1 1) than on Pt(5 5 4) surfaces. As they detect only CO_{ads} on surfaces with many low-coordination sites the authors suggest that $CH_{x,ads}$ is only stable on terrace sites, while it is quickly oxidized to CO_{ads} on (1 1 0) sites. Also, the onset potential for oxidation currents was found to be as low as 0.35 V vs. RHE for Pt(1 1 0) in alkaline media [172]. Tian et al. grew tetrahexahedral Pd Nanocrystals from electrodeposited Pd nuclei [173]. These nanocrystals predominantly feature {7 3 0} facets which are composed of two (2 1 0) steps followed by one (3 1 0) step. The authors assume that this high concentration of surface atomic steps may cause the measured 4–6-fold increase in EOR current when comparing it to commercial Pd-black in 0.1 M EtOH and 0.1 M NaOH. Furthermore the nanoparticles exhibited high stability.

For the composition of the catalyst it was found that in alkaline media the activity of Pd is slightly higher than that of Pt [49,174]. However, as for Pt in acidic media, the C—C bond cleavage is rather difficult and acetate ions are the main product [45]. Activities of Au and Ni electrodes toward the EOR were asserted to be very low, with acetate being the main product [49]. As in acidic media the addition of Sn to the catalyst was investigated for the EOR in alkaline environment [175–177]. Templated PtSn (80:20) catalysts showed a slight improvement over templated Pt catalysts [175]. As

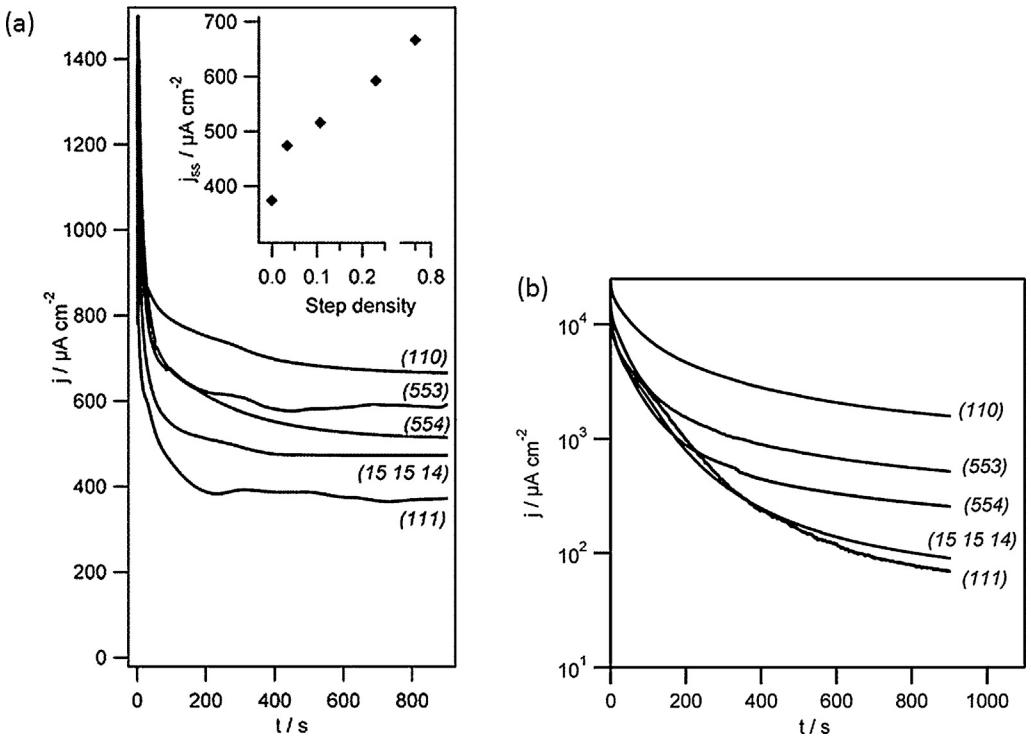

Fig. 13. Current over time transients for potential steps to 0.7 V vs. RHE. (a) Oxidation of 0.5 M EtOH in 0.1 M $HClO_4$. Inset shows the current density after 15 min over the step density. Reprinted with permission from [152], Copyright, 2008, Royal Society of Chemistry. (b) Oxidation of 0.5 M EtOH in 0.1 M NaOH. Reprinted with permission from [171], Copyright, 2009, Royal Society of Chemistry.

the observed current densities at lower potentials are higher for the PtSn catalyst it was hypothesized that that the presence of tin oxides facilitates the oxidation of adsorbed intermediates.

Antolini and Gonzalez gave an overview about studies investigating the different catalyst systems which were investigated for the EOR in alkaline media [77]. In addition to bimetallic PtM_x and PdM_x they list additions of various oxides to Pt/C and Pd/C and also catalyst systems such as RuNi without any Pd or Pt content.

Zhu et al. reported the observation of a substrate and composition effect when growing Pd on carbon-supported gold nanoparticles [178]. While the absolute EOR current is highest for pure Pd on Vulcan the current per µg Pd is highest when measured for Pd:Au ratio of 1:4. The authors attribute this to an Au induced shift of the Pd_{3d} binding energy which weakens the bonding interaction between the adsorbed species and Pd and therefore enhances the anti-poison capabilities of the catalyst [179].

Studies on the influence of the size or dispersion of catalyst nanoparticles on their activity toward EOR in alkaline media are rare. One recent publication investigates the activity of spherical Pd nanopoarticles with varying size on Ni-foil [180]. To correct for the size-dependent catalyst loading the authors converted measured currents to currents per mmol of Pd and found that nanoparticles with a diameter of 12.0 nm show a 359 times higher loading-normalized current during CV measurements than catalyst particles with a diameter of 28.8 nm. Particles with intermediate diameters (14.0 nm and 18.9 nm) followed the same trend. The authors stated that enhancement of intrinsic catalytic activity of the electrodes with smaller particles is due to an increase in 'true surface area and the availability of more energized surface Pd atoms' [180].

4.3. Catalysts at elevated temperatures

As studies coupled with spectroscopic methods, presented in Section 2, show a significant benign influence of elevated temperatures toward the total oxidation of ethanol to CO_2 the temperature effect was also studied for some model electrodes.

Jiang et al. obtained CVs for the EOR of 0.01 M EtOH in 0.1 M NaOH on Pt/C and PtSn/C at temperatures ranging from 22 to 60 °C [177]. The current density increased by a factor of 3.8 on Pt and by a factor of 1.9 on PtSn/C at 0.4 V vs. RHE for a temperature increase from 22 to 60 °C. In potentiostatic measurements the authors observed a faster deactivation of the catalyst at higher temperatures. They assume that at elevated temperatures the poisoning species (CO_{ads}) is produced faster; however, the temperature (60 °C) is not high enough to sufficiently form OH_{ads} which could oxidize the CO_{ads}.

In another study Pt/C and $Pt_{0.30}Pd_{0.38}Au_{0.32}/C$ were investigated as electrodes in 0.5 M NaOH and 1.0 M EtOH [181]. Applied temperatures ranged from 20 to 80 °C and during potentiostatic experiments a similar rapid deactivation for Pt/C was observed. $Pt_{0.30}Pd_{0.38}Au_{0.32}/C$ fared better with higher initial as well as higher long-time current densities. In Fig. 14(a) the current response to the potential steps can be seen. From the change in current density over time a long term poisoning constant δ [%/s] was calculated and the result is shown in Fig. 14(b). In contrast to Ref. [177] the poisoning rate for Pt/C decreases with increasing temperature. For $Pt_{0.30}Pd_{0.38}Au_{0.32}/C$ δ is generally lower and also decreases with increasing temperature from 40 to 80 °C. The charge density over square root of time, as depicted in Fig. 14(c), is higher for $Pt_{0.30}Pd_{0.38}Au_{0.32}/C$ than for Pt/C and increases with temperature. An analysis of the ratio of the reaction products carbonate to acetate yielded a ratio of 1.6 for Pt/C and a ratio of 1.4 for $Pt_{0.30}Pd_{0.38}Au_{0.32}/C$ at 80 °C after oxidation at a constant potential for one hour. The amount of these products was significantly larger for the ternary catalyst and the yield increased roughly linearly with temperature. The authors explain the better performance of $Pt_{0.30}Pd_{0.38}Au_{0.32}/C$ by a reduction of the activation energies by the incorporation of Pd and Au.

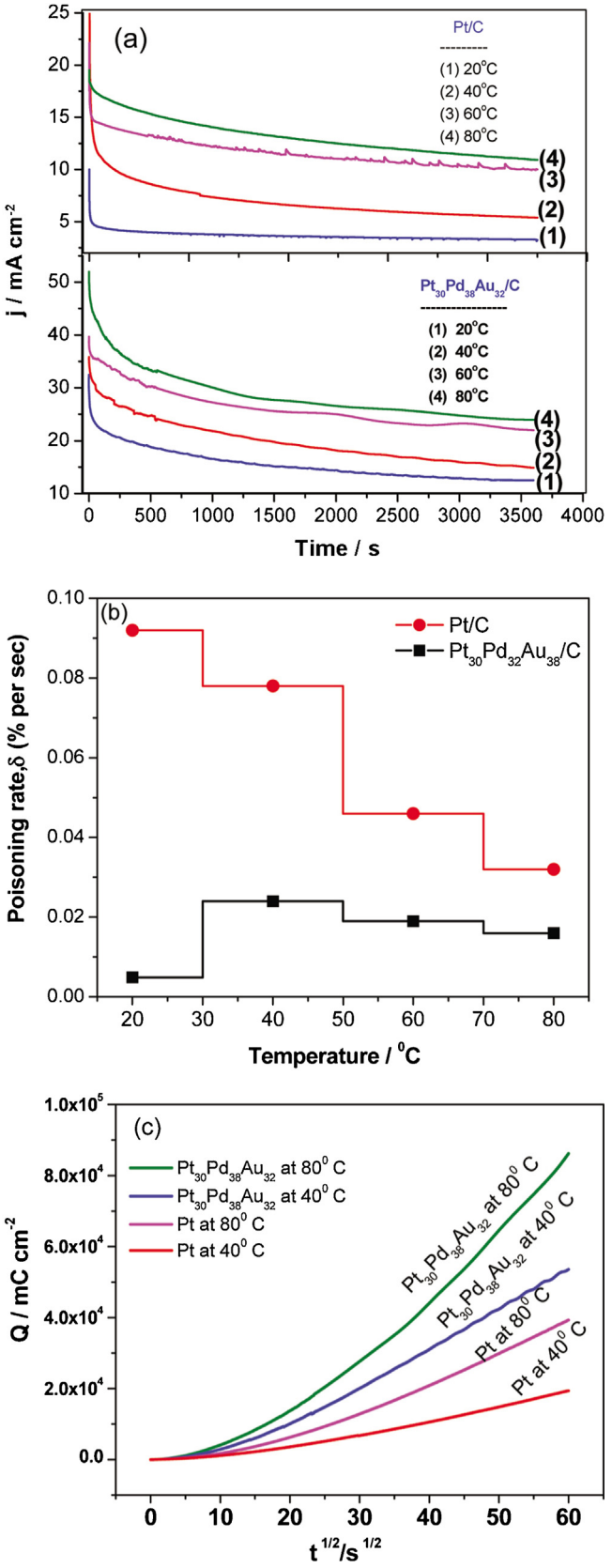

Fig. 14. (a) Potentiostatic measurement of current densities on Pt/C and $Pt_{0.30}Pd_{0.38}Au_{0.32}$/C. (b) Long term poisoning rate δ for the two catalyst systems and different temperatures. (c) Charge density over square root of time for the two catalyst systems at 40 and 80 °C. All measurements are performed in 1.0 M EtOH and 0.5 M NaOH.

Reprinted with permission from [181], Copyright 2011, American Chemical Society.

In acid solution Colmati et al. compared the performance of Pt/C, PtRu/C and Pt_3Sn/C at room temperature and in the range of 70–100 °C [182]. While both binary catalysts generated higher current densities than Pt/C, the authors demonstrated that PtRu and Pt_3Sn show a different temperature behavior. At low temperatures PtRu showed higher activity for the EOR than Pt_3Sn, while the opposite was true at higher temperatures. Colmati et al. reasoned that at low temperatures the bi-functional mechanism at PtRu supports the oxidation of CO_{ads} and CH_3CO_{ads}. At higher temperatures the electronic effect caused by the described expansion of the Pt lattice by the Sn [55] allows for faster C—C bond cleavage.

Comparing these temperature dependent studies with observations under FC conditions confirms the good activity of bimetallic PtSn catalysts [24]. With a platinum loading of 2 mg cm^{-2}, a temperature of 90 °C and an EtOH concentration of 0.1 M $Pt_{0.7}Sn_{0.3}$/Vulcan shows a CCE of approximately 74%. However, under the same conditions, Pt/Vulcan yields a CCE of roughly 72% and, as depicted in Fig. 5, at a higher catalyst loading of 8 mg cm^{-2} the CCE can be as high as 86% for Pt/Vulcan. In contrast the CCE for bimetallic PtRu catalysts was very low (<5% for 2.4 mg cm^{-2} Pt loading, T = 70 °C, EtOH concentration is 0.1 M), while the measured faradaic current densities and onset potentials are comparable to PtSn. DEMS measurements confirm that mostly AA and AAL were generated at PtRu [24,30].

Therefore, one can conclude that the oxidation of CO_{ads}, which is especially promoted by PtRu [183], is a minor challenge at elevated temperatures. To ensure a high CCE, and therefore good fuel utilization, the C—C bond scission is pivotal and can be achieved by Pt and PtSn catalysts. Apparent activation energies were determined (E_a = 53 kJ/mol for the formation of CO_2 at 0.1 M EtOH, 0.6 V vs. RHE, 5 mg cm^{-2} Pt/C [24]; E_a = 21–33 kJ/Mol for the EOR at 0.01 M EtOH, PtSn/C [177]) which in turn means that the total oxidation to CO_2 becomes more facile with higher temperatures, eventually enabling a lower load of precious metal and efficient fuel utilization.

5. Conclusions

In this present article we reviewed what is understood about the EOR reaction both in acid and alkaline media. The reaction is fairly complicated but great efforts were undertaken by many work-groups to elucidate the EOR pathways. Under fuel cell conditions CO_2 current efficiencies higher than 80% were reported in acid media [24,26,36] and higher than 50% in alkaline media [41]. A high rate of total oxidation is not only important for a high efficiency and fuel utilization but also suppresses formation of possibly toxic, undesired products such as acetaldehyde. The presented studies indicate that a DEFC should be operated at elevated temperatures to increase the kinetics of C—C bond scission. The poisonous adsorption of CO is also mitigated at higher temperatures and therefore catalysts should be mainly selected for their C—C bond splitting abilities. Membranes made from ammonium polyphosphates which can operate at intermediate temperatures seem to be promising candidates for the electrolyte due to their high ionic conductivity. In addition to increased temperature advanced catalysts could facilitate the reaction rate. For the HOR and HER fruitful interplay of theoretical and experimental work led to current densities as high as several Amperes per platinum surface on model catalysts. Comparing the model catalyst studies performed for HER and HOR to the reports for the EOR and emulating aspects which were neglected so far might lead to higher CO_2 efficiencies and enable lower loadings of precious metals. For example, the dependence of the reaction products and overall performance of the EOR, both in acid [152] and alkaline [171] media, on the different Pt basal planes Pt(1 0 0), Pt(1 1 0) and Pt(1 1 1) is understood to an extent, which is comparable to the HER/HOR [108]. Another well studied

parameter is the composition of catalysts. Especially in acid media bi-metallic PtSn was identified as catalyst with high C—C splitting activity [159]. This enhanced activity is assigned to an electronic effect which is caused by an extension of the Pt lattice parameter, similar to the increased activity of strained single Pd particles on gold surfaces toward the HER [138,139]. In addition an influence of the operation temperature on the ideal ratio of Pt: Sn was detected [155] and it was proved that only alloyed Sn shifts the Pt d-band causing an electronic effect [161]. In terms of particle size, influence of the substrate and particle dispersion results were published, however, the range of these reports is smaller than for the HOR/HER and can certainly be extended.

Apart from technical challenges for the DEFC, four key issues will decide if conversion of ethanol in a FC can emerge as one of the possible future transportation technologies: Safety, emissions, economics and sustainability [184].

In terms of safety ethanol is very benign. The liquid is non-toxic and can easily be handled. Compared to other fuels the flammability zone of ethanol is larger, 2.4–19.0 vol.% as compared to 0.6–5.6 vol.% and 1.4–7.6 vol.% for diesel fuel or gasoline, respectively. However, the flashpoint of ethanol is higher than for gasoline (286–233 K) whereas the auto-ignition temperature of ethanol is higher than the one for diesel fuel (639–503 K) [185].

When fully converting ethanol to CO_2, 2 mol of CO_2 are generated for every mole of ethanol. Simulations showed that a Mercedes-Benz A-class, a common compact car with a weight of 1150 kg, would require 3.25 l of gasoline for driving 100 km either in the new European driving cycle (NEDC) or in the city traffic of Aachen, Germany, when powered with a 50 kW FC stack with an on-board gasoline reformer [186]. The calculated system efficiency was 44%, which is partially caused by losses due to the reforming process. Assuming a system efficiency of 50% for a DEFC, 2.5 l of ethanol could propel the Mercedes-Benz A class through 100 km of one the drive cycles. This fuel consumption corresponds to an emission of 53 gCO_2 per driven kilometer. This value, which compares favorably with the emission values given in Table 1, is valid for ethanol derived from fossil fuel. In case of bio-ethanol extracted from lignocellulosic biomass the released CO_2 per driven kilometer could be as low as 3 gCO_2/km.

According to the IEA the production costs of 1 l of gasoline will rise from 0.55 USD in 2010 to 0.7 USD in 2020. For the same time interval production costs for 1 l of gasoline equivalent (LGE) for cane ethanol will stay constant at roughly 0.65 USD [2]. Addressing sustainability concerns and introducing internationally harmonized sustainability certificates should lead to a sustainable production, states the IEA in the same report. Ethanol, as a liquid fuel just like gasoline, could be distributed via the existing infrastructure. Therefore no huge investments, as for example the switch to a hydrogen economy would require, have to be put into a new supply system.

References

[1] International Energy Agency, MEDIUM-TERM Oil Market Report, 4th ed., Paris, 2009.
[2] International Energy Agency, Tracking Clean Energy Progress, Paris, 2012.
[3] G. Hoogers, 10 automotive applications, in: G. Hoogers (Ed.), Fuel Cell Technology Handbook, 1st ed., CRC Press, Washington, DC, 2003.
[4] R.S. Irani, Hydrogen storage: high-pressure gas containment, MRS Bulletin (2002) 680.
[5] J. Wolf, Liquid–hydrogen technology for vehicles, MRS Bulletin (2002) 684.
[6] R. von Helmolt, U. Eberle, Fuel cell vehicles: status 2007, Journal of Power Sources 165 (2007) 833.
[7] U. Eberle, G. Arnold, R. von Helmolt, Hydrogen storage in metal–hydrogen systems and their derivatives, Journal of Power Sources 154 (2006) 456.
[8] B. Sakintuna, F. Lamaridarkrim, M. Hirscher, Metal hydride materials for solid hydrogen storage: a review, International Journal of Hydrogen Energy 32 (2007) 1121.
[9] I.P. Jain, P. Jain, A. Jain, Novel hydrogen storage materials: a review of lightweight complex hydrides, Journal of Alloys Compounds 503 (2010) 303.
[10] J.A. Turner, Sustainable hydrogen production, Science 305 (2004) 972.
[11] H.-L. Chin, Z.-S. Chen, C.P. Chou, Fedbatch operation using clostridium acetobutylicum suspension culture as biocatalyst for enhancing hydrogen production, Biotechnology Progress 19 (2003) 383.
[12] A. Wang, N. Ren, Y. Shi, D.-J. Lee, Bioaugmented hydrogen production from microcrystalline cellulose using co-culture—clostridium acetobutylicum X9 and Ethanoigenens harbinense B49, International Journal of Hydrogen Energy 33 (2008) 912.
[13] R.J. Farrauto, From the internal combustion engine to the fuel cell: moving towards the hydrogen economy, Studies in Surface Science and Catalysis 145 (2003) 21.
[14] R. Buxbaum, H. Lei, Power output and load following in a fuel cell fueled by membrane reactor hydrogen, Journal of Power Sources 123 (2003) 43.
[15] D. Trimm, Z. Ilsen Önsan, Onboard fuel conversion for hydrogen-fuel-cell-driven vehicles, Catalysis Reviews 43 (2001) 31.
[16] Necar 5 completes first FCV cross-country trip across US, Fuel Cells Bulletin (2002).
[17] D. zur Megede, Fuel processors for fuel cell vehicles, Journal of Power Sources 106 (2002) 35.
[18] U. Stimming, Fuel cells, in: Springer Materials: Advanced Materials and Technologies, vol. 3A, Springer-Verlag, 2002, p. 228.
[19] J.R. Ladebeck, J.P. Wagner, Catalyst development for water-gas shift, in: W. Vielstich, A. Lamm, H.A. Gasteiger (Eds.), Handbook of Fuel Cells—Fundamentals, Technology and Applications, John Wiley & Sons, Ltd., Chichester, 2003, p. 190.
[20] I. Kim, O.H. Han, S.A. Chae, Y. Paik, S.-H. Kwon, K.-S. Lee, Y.E. Sung, H. Kim, Catalytic reactions in direct ethanol fuel cells, Angewandte Chemie International Edition 50 (2011) 2270.
[21] K.D. Snell, A.G. Kennan, Effect of anions and pH on the ethanol electro-oxidation at a platinum electrode, Electrochimica Acta 27 (1982) 1683.
[22] H. Hitmi, E.M. Belgsir, J.-M. Léger, C. Lamy, R.O. Lezna, A kinetic analysis of the electro-oxidation of ethanol at a platinum electrode in acid medium, Electrochimica Acta 39 (1994) 407.
[23] S. Song, W. Zhou, Z. Zhou, L. Jiang, G. Sun, Q. Xin, V. Leontidis, S. Kontou, P. Tsiakaras, Direct ethanol PEM fuel cells: the case of platinum based anodes, International Journal of Hydrogen Energy 30 (2005) 995.
[24] V. Rao, C. Cremers, U. Stimming, L. Cao, S. Sun, S. Yan, G. Sun, Q. Xin, Electro-oxidation of ethanol at gas diffusion electrodes: a DEMS study, Journal of the Electrochemical Society 154 (2007) B1138.
[25] A. Tripković, K. Popović, B. Grgur, B. Blizanac, P. Ross, N. Marković, Methanol electrooxidation on supported Pt and PtRu catalysts in acid and alkaline solutions, Electrochimica Acta 47 (2002) 3707.
[26] I. Shimada, Y. Oshima, J. Otomo, Acceleration of ethanol electro-oxidation on a carbon-supported platinum catalyst at intermediate temperatures, Journal of the Electrochemical Society 158 (2011) B369.
[27] J. Wang, S. Wasmus, R.F. Savinell, Evaluation of ethanol, 1-propanol, and 2-propanol in a direct oxidation polymer-electrolyte fuel cell, Journal of the Electrochemical Society 142 (1995) 4218.
[28] H. Wang, Z. Jusys, R.J. Behm, Ethanol electro-oxidation on carbon-supported Pt, PtRu and Pt_3Sn catalysts: a quantitative DEMS study, Journal of Power Sources 154 (2006) 351.
[29] H. Wang, Z. Jusys, R.J. Behm, Ethanol electrooxidation on a carbon-supported Pt catalyst: reaction kinetics and product yields, Journal of Physical Chemistry B 108 (2004) 19413.
[30] N. Fujiwara, K.A. Friedrich, U. Stimming, Ethanol oxidation on PtRu electrodes studied by differential electrochemical mass spectrometry, Journal of Electroanalytical Chemistry 472 (1999) 120.
[31] J. De Souza, S. Queiroz, Electro-oxidation of ethanol on Pt, Rh, and PtRh electrodes. A study using DEMS and in-situ FTIR techniques, Journal of Physical Chemistry B 106 (2002) 9825.
[32] T. Iwasita, E. Pastor, A DEMS and FTIR spectroscopic investigation of adsorbed ethanol on polycrystalline platinum, Electrochimica Acta 39 (1994) 531.
[33] L.-W.H. Leung, S.-C. Chang, M.J. Weaver, Real-time FTIR spectroscopy as an electrochemical mechanistic probe: electrooxidation of ethanol and related species on well-defined Pt (1 1 1) surfaces, Journal of Electroanalytical Chemistry 266 (1989) 317.
[34] G.A. Camara, T. Iwasita, Parallel pathways of ethanol oxidation: the effect of ethanol concentration, Journal of Electroanalytical Chemistry 578 (2005) 315.
[35] C. Lamy, S. Rousseau, E. Belgsir, C. Coutanceau, J. Leger, Recent progress in the direct ethanol fuel cell: development of new platinum–tin electrocatalysts, Electrochimica Acta 49 (2004) 3901.
[36] A.S. Aricò, P. Cretì, P.L. Antonucci, V. Antonucci, Comparison of ethanol and methanol oxidation in a liquid-feed solid polymer electrolyte fuel cell at high temperature, Electrochemical and Solid State Letters 1 (1998) 66.
[37] S. Rousseau, C. Coutanceau, C. Lamy, J.-M. Léger, Direct ethanol fuel cell (DEFC): electrical performances and reaction products distribution under operating conditions with different platinum-based anodes, Journal of Power Sources 158 (2006) 18.
[38] F. Vigier, C. Coutanceau, F. Hahn, E.M. Belgsir, C. Lamy, On the mechanism of ethanol electro-oxidation on Pt and PtSn catalysts: electrochemical and in situ IR reflectance spectroscopy studies, Journal of Electroanalytical Chemistry 563 (2004) 81.
[39] M. Watanabe, S. Motoo, Part III. Enhancement of the oxidation of carbon monoxide on platinum by ruthenium Ad-atoms, Journal of Electroanalytical Chemistry 60 (1975) 275.
[40] Y. Morimoto, E. Yeager, CO oxidation on smooth and high area Pt, Pt–Ru and Pt–Sn electrodes, Journal of Electroanalytical Chemistry 441 (1998) 77.

[41] V. Rao, C. Cremers, U. Stimming, Investigation of the ethanol electro-oxidation in alkaline membrane electrode assembly by differential electrochemical mass spectrometry, Fuel Cells 7 (2007) 417.
[42] A.A. Abd-El-Latif, E. Mostafa, S. Huxter, G. Attard, H. Baltruschat, Electrooxidation of ethanol at polycrystalline and platinum stepped single crystals: a study by differential electrochemical mass spectrometry, Electrochimica Acta 55 (2010) 7951.
[43] A. Tripković, K. Popović, J. Lović, The influence of the oxygen-containing species on the electrooxidation of the C1–C4 alcohols at some platinum single crystal surfaces in alkaline solution, Electrochimica Acta 46 (2001) 3163.
[44] G. Cui, S. Song, P. Shen, A. Kowal, C. Bianchini, First-principles considerations on catalytic activity of Pd toward ethanol oxidation, Journal of Physical Chemistry C 113 (2009) 15639.
[45] Z.X. Liang, T.S. Zhao, J.B. Xu, L.D. Zhu, Mechanism study of the ethanol oxidation reaction on palladium in alkaline media, Electrochimica Acta 54 (2009) 2203.
[46] N. Fujiwara, Z. Siroma, S. Yamazaki, T. Ioroi, H. Senoh, K. Yasuda, Direct ethanol fuel cells using an anion exchange membrane, Journal of Power Sources 185 (2008) 621.
[47] X. Fang, L. Wang, P.K. Shen, G. Cui, C. Bianchini, An in situ Fourier transform infrared spectroelectrochemical study on ethanol electrooxidation on Pd in alkaline solution, Journal of Power Sources 195 (2010) 1375.
[48] Z.-Y. Zhou, Q. Wang, J.-L. Lin, N. Tian, S.-G. Sun, In situ FTIR spectroscopic studies of electrooxidation of ethanol on Pd electrode in alkaline media, Electrochimica Acta 55 (2010) 7995.
[49] D. Bayer, C. Cremers, H. Baltruschat, J. Tübke, The electro-oxidation of ethanol in alkaline medium at different catalyst metals, ECS Transactions 41 (2011) 1669.
[50] D. Bayer, S. Berenger, M. Joos, C. Cremers, J. Tübke, Electrochemical oxidation of C2 alcohols at platinum electrodes in acidic and alkaline environment, International Journal of Hydrogen Energy 35 (2010) 12660.
[51] A. Santasalo-Aarnio, Y. Kwon, E. Ahlberg, K. Kontturi, T. Kallio, M.T.M. Koper, Comparison of methanol, ethanol and iso-propanol oxidation on Pt and Pd electrodes in alkaline media studied by HPLC, Electrochemistry Communications 13 (2011) 466.
[52] S.Y. Shen, T.S. Zhao, Q.X. Wu, Product analysis of the ethanol oxidation reaction on palladium-based catalysts in an anion-exchange membrane fuel cell environment, International Journal of Hydrogen Energy 37 (2012) 575.
[53] D. Bayer, C. Cremers, H. Baltruschat, J. Tübke, Ethanol stripping in alkaline medium: a DEMS study, ECS Transactions 25 (2010) 85.
[54] C. Bianchini, P.K. Shen, Palladium-based electrocatalysts for alcohol oxidation in half cells and in direct alcohol fuel cells, Chemical Reviews 109 (2009) 4183.
[55] P.E. Tsiakaras, PtM/C (M = Sn, Ru, Pd, W) based anode direct ethanol–PEMFCs: structural characteristics and cell performance, Journal of Power Sources 171 (2007) 107.
[56] T. Norby, Solid-state protonic conductors: principles, properties, progress and prospects, Solid State Ionics 125 (1999) 1.
[57] N.H. Jalani, K. Dunn, R. Datta, Synthesis and characterization of Nafion®-MO_2 (M = Zr, Si, Ti) nanocomposite membranes for higher temperature PEM fuel cells, Electrochimica Acta 51 (2005) 553.
[58] B. Zhu, I. Albinsson, B. Mellander, G. Meng, Intermediate-temperature proton-conducting fuel cells—present experience and future opportunities, Solid State Ionics 125 (1999) 439.
[59] B. Zhu, Intermediate temperature proton conducting salt–oxide composites, Solid State Ionics 125 (1999) 397.
[60] A.I. Baranov, V.M. Duda, D.J. Jones, J. Roziere, Hydrogen insertion and protonic conductivity in lead, Solid State Ionics (2001) 241.
[61] T.S. Zhang, S.H. Chan, L.B. Kong, P.T. Sheng, J. Ma, Synergetic effect of NiO and SiO_2 on the sintering and properties of 8 mol% yttria-stabilized zirconia electrolytes, Electrochimica Acta 54 (2009) 927.
[62] B.C.H. Steele, Appraisal of $Ce_{(1-y)}Gd_yO_{(2-y/2)}$ electrolytes for IT-SOFC operation at 500 °C, Solid State Ionics 129 (2000) 95.
[63] J. Otomo, N. Minagawa, C. Wen, K. Eguchi, H. Takahashi, Protonic conduction of CsH_2PO_4 and its composite with silica in dry and humid atmospheres, Solid State Ionics 156 (2003) 357.
[64] J. Otomo, S. Nishida, H. Takahashi, H. Nagamoto, Electro-oxidation of methanol and ethanol on carbon-supported Pt catalyst at intermediate temperature, Journal of Electroanalytical Chemistry 615 (2008) 84.
[65] Y. Jiang, T. Matthieu, R. Lan, X. Xu, P.I. Cowin, S. Tao, A stable NH_4PO_3-glass proton conductor for intermediate temperature fuel cells, Solid State Ionics 192 (2011) 108.
[66] M. Cappadonia, O. Niemzig, Preliminary study on the ionic conductivity of a polyphosphate composite, Solid State Ionics 125 (1999) 333.
[67] S. Haufe, D. Prochnow, D. Schneider, O. Geier, D. Freude, U. Stimming, Polyphosphate composite: conductivity and NMR studies, Solid State Ionics 176 (2005) 955.
[68] T. Kenjo, Y. Ogawa, Proton conductors based on ammonium polyphosphate, Solid State Ionics 76 (1995) 29.
[69] T. Matsui, S. Takeshita, Y. Iriyama, T. Abe, M. Inaba, Z. Ogumi, Proton conductivity of $(NH_4)_2TiP_4O_{13}$-based material for intermediate temperature fuel cells, Electrochemistry Communications 6 (2004) 180.
[70] T. Matsui, S. Takeshita, Y. Iriyama, T. Abe, Z. Ogumi, Correlation between electrochemical and structural properties in $NH_4PO_3/(NH_4)_2MP_4O_{13}$ (M = Ti and Si) composites at intermediate temperatures, Solid State Ionics 178 (2007) 859.
[71] H. Wang, C. Tealdi, U. Stimming, K. Huang, L. Chen, Preparation and conductivity measurements of ammonium polyphosphate-based proton conductors, Electrochimica Acta 54 (2009) 5257.
[72] C. Sun, U. Stimming, Synthesis and characterization of NH_4PO_3 based composite with superior proton conductivity for intermediate temperature fuel cells, Electrochimica Acta 53 (2008) 6417.
[73] L. Liu, H. Tu, C. Cremers, U. Stimming, NH_4PO_3/SiO_2 composite as electrolyte for intermediate temperature fuel cells, Solid State Ionics 177 (2006) 2417.
[74] N. Kluy, B.B.L. Reeb, O. Paschos, F. Maglia, O. Schneider, U. Stimming, et al., Ammonium polyphosphate composite based electrolytes for intermediate temperature fuel cells, in: Proceedings of the 222nd Meeting of the Electrochemical Society, Honolulu, HI, 2012.
[75] G. Merle, M. Wessling, K. Nijmeijer, Anion exchange membranes for alkaline fuel cells: a review, Journal of Membrane Science 377 (2011) 1.
[76] T.S. Zhao, Y.S. Li, S.Y. Shen, Anion-exchange membrane direct ethanol fuel cells: status and perspective, Frontiers of Energy and Power Engineering in China 4 (2010) 443.
[77] E. Antolini, E.R. Gonzalez, Alkaline direct alcohol fuel cells, Journal of Power Sources 195 (2010) 3431.
[78] J.R. Varcoe, R.C.T. Slade, Prospects for alkaline anion-exchange membranes in low temperature fuel cells, Fuel Cells 5 (2005) 187.
[79] B. Hammer, J.K. Nørskov, Electronic factors determining the reactivity of metal surfaces, Surface Science 343 (1995) 211.
[80] S. Trasatti, Work function, electronegativity, and electrochemical behaviour of metals, Journal of Electroanalytical Chemistry 39 (1972) 163.
[81] B.E. Conway, J.O. Bockris, Electrolytic hydrogen evolution kinetics and its relation to the electronic and adsorptive properties of the metal, Journal of Chemical Physics 26 (1957) 532.
[82] R. Parsons, The rate of electrolytic hydrogen evolution and the heat of adsorption of hydrogen, Transactions on Faraday Society 54 (1958) 1053.
[83] J. Greeley, J.K. Nørskov, L.A. Kibler, A.M. El-Aziz, D.M. Kolb, Hydrogen evolution over bimetallic systems: understanding the trends, ChemPhysChem 7 (2006) 1032.
[84] S. Pandelov, U. Stimming, Reactivity of monolayers and nano-islands of palladium on Au(1 1 1) with respect to proton reduction, Electrochimica Acta 52 (2007) 5548.
[85] J. Greeley, T.F. Jaramillo, J. Bonde, I.B. Chorkendorff, J.K. Nørskov, Computational high-throughput screening of electrocatalytic materials for hydrogen evolution, Nature Materials 5 (2006) 909.
[86] J.K. Nørskov, T. Bligaard, A. Logadottir, J.R. Kitchin, J.G. Chen, S. Pandelov, U. Stimming, Trends in the exchange current for hydrogen evolution, Journal of the Electrochemical Society 152 (2005) J23.
[87] K. Friedrich, F. Henglein, U. Stimming, W. Unkauf, Size dependence of the CO monolayer oxidation on nanosized Pt particles supported on gold, Electrochimica Acta 45 (2000) 3283.
[88] F. Maillard, M. Eikerling, O.V. Cherstiouk, S. Schreier, E. Savinova, U. Stimming, Size effects on reactivity of Pt nanoparticles in CO monolayer oxidation: the role of surface mobility, Faraday Discussions 125 (2004) 357.
[89] F. Maillard, E.R. Savinova, U. Stimming, CO monolayer oxidation on Pt nanoparticles: further insights into the particle size effects, Journal of Electroanalytical Chemistry 599 (2007) 221.
[90] H.A. Gasteiger, J.E. Panels, S.G. Yan, Dependence of PEM fuel cell performance on catalyst loading, Journal of Power Sources 127 (2004) 162.
[91] K.C. Neyerlin, W. Gu, J. Jorne, H.A. Gasteiger, Study of the exchange current density for the hydrogen oxidation and evolution reactions, Journal of the Electrochemical Society 154 (2007) B631.
[92] F. Hernandez, H. Baltruschat, Hydrogen evolution and Cu UPD at stepped gold single crystals modified with Pd, Journal of Solid State Electrochemistry 11 (2007) 877.
[93] F. Hernandez, H. Baltruschat, Electrochemical characterization of gold stepped surfaces modified with Pd, Langmuir 22 (2006) 4877.
[94] V. Del Colle, A. Berna, G. Tremiliosi-Filho, E. Herrero, J.M. Feliu, Electrocatalysis: theory and experiment at the interface, Physical Chemistry Chemical Physics 10 (2008) 3607.
[95] Y. Zhou, R. Pasquarelli, T. Holme, J. Berry, D. Ginley, R. O'Hayre, Improving PEM fuel cell catalyst activity and durability using nitrogen-doped carbon supports: observations from model Pt/HOPG systems, Journal of Materials Chemistry 19 (2009) 7830.
[96] A. Roudgar, A. Groß, Local reactivity of metal overlayers: density functional theory calculations of Pd on Au, Physical Review B 67 (2003) 2.
[97] A. Roudgar, A. Groß, Local reactivity of thin Pd overlayers on Au single crystals, Journal of Electroanalytical Chemistry 548 (2003) 121.
[98] J. Kitchin, J. Nørskov, M. Barteau, J. Chen, Role of strain and ligand effects in the modification of the electronic and chemical properties of bimetallic surfaces, Physical Review Letters 93 (2004) 4.
[99] L.A. Kibler, A.M. El-Aziz, R. Hoyer, D.M. Kolb, Tuning reaction rates by lateral strain in a palladium monolayer, Angewandte Chemie International Edition 44 (2005) 2080.
[100] H. Wolfschmidt, D. Weingarth, U. Stimming, Enhanced reactivity for hydrogen reactions at Pt nanoislands on Au(1 1 1), ChemPhysChem 11 (2010) 1533.
[101] S. Chen, A. Kucernak, Electrocatalysis under conditions of high mass transport rate: oxygen reduction on single submicrometer-sized Pt particles supported on carbon, Journal of Physical Chemistry B 108 (2004) 3262.
[102] P.M. Quaino, J.L. Fernández, M.R. Gennero de Chialvo, A.C. Chialvo, Hydrogen oxidation reaction on microelectrodes: analysis of the contribution of the kinetic routes, Journal of Molecular Catalysis A: Chemical 252 (2006) 156.

[103] N.M. Marković, S.T. Sarraf, H.A. Gasteiger, P.N. Ross Jr., Hydrogen electrochemistry on platinum low-index single-crystal surfaces in alkaline solution, Faraday Transactions 92 (1996) 3719.
[104] J. Barber, S. Morin, B.E. Conway, Specificity of the kinetics of H_2 evolution to the structure of single-crystal Pt surfaces, and the relation between opd and upd H, Journal of Electroanalytical Chemistry 446 (1998) 125.
[105] F. Gloaguen, J.M. Leger, C. Lamy, A. Marmann, U. Stimming, R. Vogel, Platinum electrodeposition on graphite: electrochemical study and STM imaging, Electrochimica Acta 44 (1999) 1805.
[106] T. Brülle, U. Stimming, Platinum nanostructured HOPG—preparation, characterization and reactivity, Journal of Electroanalytical Chemistry 636 (2009) 10.
[107] N.M. Marković, P.N. Ross Jr., Surface science studies of model fuel cell electrocatalysts, Surface Science Reports 45 (2002) 117.
[108] N.M. Marković, B.N. Grgur, P.N. Ross, Temperature-dependent hydrogen electrochemistry on platinum low-index single-crystal surfaces in acid solutions, Journal of Physical Chemistry B 27 (1997) 5405.
[109] J. Perez, E.R. Gonzalez, H.M. Villullas, Hydrogen evolution reaction on gold single-crystal electrodes in acid solutions, Journal of Physical Chemistry B 102 (1998) 10931.
[110] M. Baldauf, D.M. Kolb, A hydrogen adsorption and absorption study with ultrathin Pd overlayers on Au(1 1 1) and Au(1 0 0), Electrochimica Acta 38 (1993) 2145.
[111] H. Naohara, S. Ye, K. Uosaki, Electrocatalytic reactivity for oxygen reduction at epitaxially grown Pd thin layers of various thickness on Au (1 1 1) and Au (1 0 0), Electrochimica Acta 45 (2000) 3305.
[112] L.A. Kibler, A. El-Aziz, D. Kolb, Electrochemical behaviour of pseudomorphic overlayers: Pd on Au(1 1 1), Journal of Molecular Catalysis A: Chemical 199 (2003) 57.
[113] B. Hammer, J.B. Nørskov, Theoretical surface science and catalysis—calculations and concepts, Advances in Catalysis 45 (2000).
[114] W.B. Wang, M.S. Zei, G. Ertl, Electrooxidation of CO on Ru (0 0 0 1) and RuO_2 (1 0 0) electrode surfaces, Chemical Physics Letters 355 (2002) 301.
[115] W.B. Wang, M.S. Zei, G. Ertl, Electrosorption and electrooxidation of CO on Ru (0 0 0 1), Physical Chemistry Chemical Physics 3 (2001) 3307.
[116] H.H. Wolfschmidt, Interfaces and Energy Conversion Substrate Effects in Electrocatalysis, PhD Thesis, Technische Universitaet Muenchen, 2012.
[117] J.V. Zoval, R.M. Stiger, P.R. Biernacki, R.M. Penner, Electrochemical deposition of silver nanocrystallites on the atomically smooth graphite basal plane, Journal of Physical Chemistry 100 (1996) 837.
[118] G. Kästle, H.-G. Boyen, F. Weigl, P. Ziemann, S. Riethmüller, C.H. Hartmann, J.P. Spatz, M. Möller, M.G. Garnier, P. Oelhafen, The self-organization of metal loaded micelles—an approach to prepare ordered arrays of metallic nanoislands, Phase Transitions 76 (2003) 307.
[119] P. Eibeck, J.P. Spatz, S. Moessmer, M. Moeller, H. Herzog, P. Ziemann, Nanostructuring by ultrathin diblock copolymer/titanium composite films, Nanostructured Materials 12 (1999) 383.
[120] M. Hiramatsu, M. Hori, preparation of dispersed platinum nanoparticles on a carbon nanostructured surface using supercritical fluid chemical deposition, Materials 3 (2010) 1559.
[121] D.M. Kolb, F.C. Simeone, Nanostructure formation at the solid/liquid interface, Current Opinion in Solid State and Materials Science 9 (2005) 91.
[122] D.M. Kolb, F.C. Simeone, Electrochemical nanostructuring with an STM: a status report, Electrochimica Acta 50 (2005) 2989.
[123] W. Li, J. Virtanen, R. Penner, A nanometer-scale galvanic cell, Journal of Physical Chemistry 96 (1992) 6529.
[124] R.M. Nyffenegger, R.M. Penner, Nanometer-scale surface modification using the scanning probe microscope: progress since 1991, Chemical Reviews 97 (1997) 1195.
[125] M. Petri, D.M. Kolb, Nanostructuring of a sodium dodecyl sulfate-covered Au(1 1 1) electrode, Physical Chemistry Chemical Physics 4 (2002) 1211.
[126] D.M. Kolb, Nanofabrication of small copper clusters on gold(1 1 1) electrodes by a scanning tunneling microscope, Science 275 (1997) 1097.
[127] G. Engelmann, J. Ziegler, D. Kolb, Electrochemical fabrication of large arrays of metal nanoclusters, Surface Science 401 (1998) L420.
[128] M. Del Pópolo, E.P.M. Leiva, H. Kleine, J. Meier, U. Stimming, M. Mariscal, W. Schmickler, A combined experimental and theoretical study of the generation of palladium clusters on Au(1 1 1) with a scanning tunnelling microscope, Electrochimica Acta 48 (2003) 1287.
[129] D.M. Kolb, Electrochemical surface science, Angewandte Chemie International Edition 40 (2001) 1162.
[130] J. Ustarroz, X. Ke, A. Hubin, S. Bals, H. Terryn, New insights into the early stages of nanoparticle electrodeposition, Journal of Physical Chemistry C 116 (2012) 2322.
[131] M.E. Hyde, R.G. Compton, A review of the analysis of multiple nucleation with diffusion controlled growth, Journal of Electroanalytical Chemistry 549 (2003) 1.
[132] J. Zoval, J. Lee, S. Gorer, Electrochemical preparation of platinum nanocrystallites with size selectivity on basal plane oriented graphite surfaces, Journal of Physical Chemistry 5647 (1998) 1166.
[133] J.L. Fransaer, R.M. Penner, Brownian dynamics simulation of the growth of metal nanocrystal ensembles on electrode surfaces from solution. I. Instantaneous nucleation and diffusion-controlled growth, Journal of Physical Chemistry B 103 (1999) 7643.
[134] R.M. Penner, Brownian dynamics simulations of the growth of metal nanocrystal ensembles on electrode surfaces in solution. 2. The effect of deposition rate on particle size, Journal of Physical Chemistry B 105 (2001) 8672.
[135] H. Liu, F. Favier, K. Ng, M. Zach, R. Penner, Size-selective electrodeposition of meso-scale metal particles: a general method, Electrochimica Acta 47 (2001) 671.
[136] M. Ueda, H. Dietz, A. Anders, H. Kneppe, A. Meixner, W. Plieth, Double-pulse technique as an electrochemical tool for controlling the preparation of metallic nanoparticles, Electrochimica Acta 48 (2002) 377.
[137] T. Brülle, A. Denisenko, H. Sternschulte, U. Stimming, Catalytic activity of platinum nanoparticles on highly boron-doped and 1 0 0-oriented epitaxial diamond towards HER and HOR, Physical Chemistry Chemical Physics 13 (2011) 12883.
[138] J. Meier, J. Schiøtz, P. Liu, J.K. Nørskov, U. Stimming, Nano-scale effects in electrochemistry, Chemical Physics Letters 390 (2004) 440.
[139] J. Meier, K.A. Friedrich, U. Stimming, Novel method for the investigation of single nanoparticle reactivity, Faraday Discussions 121 (2002) 365.
[140] A. Ruban, B. Hammer, P. Stoltze, H.L. Skriver, J.K. Nørskov, Surface electronic structure and reactivity of transition and noble metals, Journal of Molecular Catalysis A: Chemical (1997) 421.
[141] A. Ruban, H. Skriver, J. Nørskov, Surface segregation energies in transition-metal alloys, Physical Review B 59 (1999) 990.
[142] M. Mavrikakis, B. Hammer, J.K. Nørskov, Effect of strain on the reactivity of metal surfaces, Physical Review Letters 81 (1998) 2819.
[143] L.A. Kibler, Hydrogen electrocatalysis, ChemPhysChem 7 (2006) 985.
[144] H. Wolfschmidt, R. Bussar, U. Stimming, Charge transfer reactions at nanostructured Au(1 1 1) surfaces: influence of the substrate material on electrocatalytic activity, Journal of Physical Chemistry B: Condensed Matter 20 (2008) 374127.
[145] M. Eikerling, J. Meier, U. Stimming, Hydrogen evolution at a single supported nanoparticle: a kinetic model, Zeitschrift fur Physikalische Chemie 217 (2003) 395.
[146] T. Mitsui, M.K. Rose, E. Fomin, D.F. Ogletree, M. Salmeron, Hydrogen adsorption and diffusion on Pd(1 1 1), Surface Science 540 (2003) 5.
[147] T. Löffler, R. Bussar, E. Drbalkova, P. Janderka, H. Baltruschat, The role of mono-atomic steps and of step decoration by Cu on the adsorption and hydrogenation of benzene and cyclohexene on Pt single crystal electrodes, Electrochimica Acta 48 (2003) 3829.
[148] X.H. Xia, H.-D. Liess, T. Iwasita, Early stages in the oxidation of ethanol at low index single crystal platinum electrodes, Journal of Electroanalytical Chemistry 437 (1997) 233.
[149] J. Shin, W.J. Tornquist, C. Korzeniewski, C.S. Hoaglund, Elementary steps in the oxidation and dissociative chemisorption of ethanol on smooth and stepped surface planes of platinum electrodes, Surface Science 364 (1996) 122.
[150] F. Colmati, G. Tremiliosi-Filho, E.R. Gonzalez, A. Berná, E. Herrero, J.M. Feliu, Surface structure effects on the electrochemical oxidation of ethanol on platinum single crystal electrodes, Faraday Discussions 140 (2009) 9.
[151] F. Colmati, G. Tremiliosi-Filho, E.R. Gonzalez, A. Berná, E. Herrero, J.M. Feliu, The role of the steps in the cleavage of the C—C bond during ethanol oxidation on platinum electrodes, Physical Chemistry Chemical Physics 11 (2009) 9114.
[152] S.C.S. Lai, M.T.M. Koper, Electro-oxidation of ethanol and acetaldehyde on platinum single-crystal electrodes, Faraday Discussions 140 (2009) 399.
[153] J. Mostany, E. Herrero, Thermodynamic studies of anion adsorption at stepped platinum($h\,k\,l$) electrode surfaces in sulfuric acid solutions, Journal of Physical Chemistry B 106 (2002) 12787.
[154] H.-F. Wang, Z.-P. Liu, Comprehensive mechanism and structure-sensitivity of ethanol oxidation on platinum: new transition-state searching method for resolving the complex reaction network, Journal of the American Chemical Society 130 (2008) 10996.
[155] E. Antolini, E.R. Gonzalez, Effect of synthesis method and structural characteristics of Pt–Sn fuel cell catalysts on the electro-oxidation of CH_3OH and CH_3CH_2OH in acid medium, Catalysis Today 160 (2011) 28.
[156] S. Zignani, E. Gonzalez, Investigation of a Pt_3Sn/C electro-catalyst in a direct ethanol fuel cell operating at low temperatures for portable applications, International Journal of Electrochemical Science 7 (2012) 3155.
[157] W.J. Zhou, S.Q. Song, W.Z. Li, Z.H. Zhou, G.Q. Sun, Q. Xin, S. Douvartzides, P. Tsiakaras, Direct ethanol fuel cells based on PtSn anodes: the effect of Sn content on the fuel cell performance, Journal of Power Sources 140 (2005) 50.
[158] J.H. Kim, S.M. Choi, S.H. Nam, M.H. Seo, S.H. Choi, W.B. Kim, Influence of Sn content on PtSn/C catalysts for electrooxidation of C1–C3 alcohols: synthesis, characterization, and electrocatalytic activity, Applied Catalysis B-Environmental 82 (2008) 89.
[159] S. García-Rodríguez, F. Somodi, I. Borbáth, J.L. Margitfalvi, M.A. Peña, J.L.G. Fierro, S. Rojas, Controlled synthesis of Pt–Sn/C fuel cell catalysts with exclusive Sn–Pt interaction, Applied Catalysis B-Environmental 91 (2009) 83.
[160] P. Liu, A. Logadottir, J.K. Nørskov, Modeling the electro-oxidation of CO and H_2/CO on Pt, Ru, PtRu and Pt_3Sn, Electrochimica Acta 48 (2003) 3731.
[161] D.R.M. Godoi, J. Perez, H.M. Villullas, Alloys and oxides on carbon-supported Pt–Sn electrocatalysts for ethanol oxidation, Journal of Power Sources 195 (2010) 3394.
[162] L. Jiang, L. Colmenares, Z. Jusys, G.Q. Sun, R.J. Behm, Ethanol electrooxidation on novel carbon supported Pt/SnO_x/C catalysts with varied Pt:Sn ratio, Electrochimica Acta 53 (2007) 377.
[163] F. Colmati, E. Antolini, E.R. Gonalez, Ethanol oxidation on carbon supported Pt–Sn electrocatalysts prepared by reduction with formic acid, Journal of the Electrochemical Society 154 (2007) B39.

[164] J.E. Thomas, A.R. Bonesi, M.S. Moreno, A. Visintin, A.M. Castro Luna, W.E. Triaca, Carbon nanotubes as catalyst supports for ethanol oxidation, International Journal of Hydrogen Energy 35 (2010) 11681.
[165] L. Dong, R.R.S. Gari, Z. Li, M.M. Craig, S. Hou, Graphene-supported platinum and platinum–ruthenium nanoparticles with high electrocatalytic activity for methanol and ethanol oxidation, Carbon 48 (2010) 781.
[166] Y. Yao, Q. Fu, Z. Zhang, H. Zhang, T. Ma, D. Tan, X. Bao, Structure control of Pt–Sn bimetallic catalysts supported on highly oriented pyrolytic graphite (HOPG), Applied Surface Science 254 (2008) 3808.
[167] A.A. El-Shafei, M. Eiswirth, Electrochemical activity of Sn-modified Pt single crystal electrodes for ethanol oxidation, Surface Science 604 (2010) 862.
[168] Q.-W. Zheng, C.-J. Fan, C.-H. Zhen, Z.-Y. Zhou, S.-G. Sun, Irreversible adsorption of Sn adatoms on basal planes of Pt single crystal and its impact on electrooxidation of ethanol, Electrochimica Acta 53 (2008) 6081.
[169] L. Colmenares, H. Wang, Z. Jusys, L. Jiang, S. Yan, G.Q. Sun, J.J. Behm, Ethanol oxidation on novel, carbon supported Pt alloy catalysts—model studies under defined diffusion conditions, Electrochimica Acta 52 (2006) 221.
[170] J. Perez, V.A. Paganin, E. Antolini, Particle size effect for ethanol electrooxidation on Pt/C catalysts in half-cell and in a single direct ethanol fuel cell, Journal of Electroanalytical Chemistry 654 (2011) 108.
[171] S.C.S. Lai, M.T.M. Koper, Ethanol electro-oxidation on platinum in alkaline media, Physical Chemistry Chemical Physics 11 (2009) 10446.
[172] J.S. Spendelow, A. Wieckowski, Electrocatalysis of oxygen reduction and small alcohol oxidation in alkaline media, Physical Chemistry Chemical Physics 9 (2007) 2654.
[173] N. Tian, Z.-Y. Zhou, N.-F. Yu, L.-Y. Wang, S.-G. Sun, Direct electrodeposition of tetrahexahedral Pd nanocrystals with high-index facets and high catalytic activity for ethanol electrooxidation, Journal of the American Chemical Society 132 (2010) 7580.
[174] C. Xu, L. Cheng, P. Shen, Y. Liu, Methanol and ethanol electrooxidation on Pt and Pd supported on carbon microspheres in alkaline media, Electrochemistry Communications 9 (2007) 997.
[175] E.E. Switzer, T.S. Olson, A.K. Datye, P. Atanassov, M.R. Hibbs, C.J. Cornelius, Templated Pt–Sn electrocatalysts for ethanol, methanol and CO oxidation in alkaline media, Electrochima Acta 54 (2009) 989.
[176] Q. He, W. Chen, S. Mukerjee, S. Chen, F. Laufek, Carbon-supported PdM (M = Au and Sn) nanocatalysts for the electrooxidation of ethanol in high pH media, Journal of Power Sources 187 (2009) 298.
[177] L. Jiang, A. Hsu, D. Chu, R. Chen, Ethanol electro-oxidation on Pt/C and PtSn/C catalysts in alkaline and acid solutions, International Journal of Hydrogen Energy 35 (2010) 365.
[178] L.D. Zhu, T.S. Zhao, J.B. Xu, Z.X. Liang, Preparation and characterization of carbon-supported sub-monolayer palladium decorated gold nanoparticles for the electro-oxidation of ethanol in alkaline media, Journal of Power Sources 187 (2009) 80.
[179] D.I. Enache, J.K. Edwards, P. Landon, B. Solsona-Espriu, A.F. Carley, A.A. Herzing, M. Watanabe, C.J. Kiely, D.W. Knight, G.J. Hutchings, Solvent-free oxidation of primary alcohols to aldehydes using Au–Pd/TiO_2 catalysts, Science 311 (2006) 362.
[180] P.S. Roy, J. Bagchi, S.K. Bhattacharya, The size-dependent anode-catalytic activity of nickel-supported palladium nanoparticles for ethanol alkaline fuel cells, Catalysis Science & Technology 2 (2012) 2302.
[181] J. Datta, A. Dutta, S. Mukherjee, The beneficial role of the cometals pd and au in the carbon-supported PtPdAu catalyst toward promoting ethanol oxidation kinetics in alkaline fuel cells: temperature effect and reaction mechanism, Journal of Physical Chemistry C 115 (2011) 15324.
[182] F. Colmati, E. Antolini, E.R. Gonzalez, Effect of temperature on the mechanism of ethanol oxidation on carbon supported Pt, PtRu and Pt_3Sn electrocatalysts, Journal of Power Sources 157 (2006) 98.
[183] H. Li, G. Sun, L. Cao, L. Jiang, Q. Xin, Comparison of different promotion effect of PtRu/C and PtSn/C electrocatalysts for ethanol electro-oxidation, Electrochimica Acta 52 (2007) 6622.
[184] K. Adamson, Hydrogen and methanol: a comparison of safety, economics, efficiencies and emissions, Journal of Power Sources (2000) 548.
[185] M.R. Brooks, D.A. Crowl, Flammability envelopes for methanol, ethanol, acetonitrile and toluene, Journal of Loss Prevention in the Process Industries 20 (2007) 144.
[186] K. Fischer, M. Rzepka, U. Stimming, J.-W. Biermann, M. Johannaber, H. Wallentowitz, Performance of gasoline fuel cell cars—a simulation study, Proceedings of the Institution of Mechanical Engineers Part D 219 (2005) 889.